Faculty of Mechanical Engineering and Informatics

Institutional Department of Machine Tools

Master of Science Thesis

Dynamical Simulation of a Robotic Structure

FELIX, Bernard Khawan

(CAATHW)

Supervisor: Dr. Szilágyi Attila

Consultant: Thomas Alves da Silva Wallyson

30th April, 2021

Declaration of Authorship

I, FELIX Bernard Khawan; Neptun-code: CAATHW, MSc. student of the Faculty of Mechanical Engineering and Informatics, University of Miskolc, being acutely aware of my legal liability, hereby confirm, declare and certify with my signature, that the thesis, entitled "Dynamical simulation of a robotic structure" –except where indicated by referencing –, is my own work, is not copied from any other person's work, and is not previously submitted for assessment at University of Miskolc or elsewhere, and all sources (both the electronic and printed literature, or any kind) referred to in it, have been used in accordance with the rules of copyright.

I understand that a thesis work may be considered to be plagiarized if it consists of

• Quoting word by word or referring to literature either with no quotation marks or no proper citation;

• Referring to content without indicating the source of references;

• Representing previously published ideas as one's own.

I, hereby declare that I have been informed of the terms of plagiarism, and I understand that in the case of plagiarism my thesis work is rejected.

Miskolc, 30th April, 2021

Student's signature

UNIVERSITY OF MISKOLC
FACULTY OF MECHANICAL ENGINEERING AND INFORMATICS

Mechanical Engineering MSc CAD/CAM specialization	1735 UNIVERSITAS MISKOLCINENSIS	№: SZG-2020/21-2-01M-a **Institutional Department of Machine Tools** 3515 Miskolc-Egyetemváros

THESIS WORK

FELIX, BERNARD KHAWAN

Neptun code: CAATHW

for mechanical engineer candidate

THESIS SUBJECT: **Simulation of Manufacturing Devices**

THESIS TITLE: **Dynamical simulation of a robotic structure**

SPECIFICATION OF PROJECT:

1. Study the dynamical properties of modern CNC robotic machining centers. Perform a detailed literature review in order to present the most frequent methods of revealing the dynamical behavior of such robotic devices.
2. Reveal and analyze the main vibrational sources of the considered manufacturing device. Set up dynamical models for the investigation the dynamic features of such devices. Compose a manual model with distributed parameters to calculate the transversal natural frequencies of one of the arms of the robotic structure.
3. Prepare the sufficiently detailed 3D digital prototype of the investigated robotic device within the frames of an integrated engineering modelling environment.
4. Applying the 3D model prepared under the previous point, create an FEM dynamical analysis and calculations in order to obtain a detailed overview on the vibrational features of the investigated manufacturing device.
5. Draw some conclusions on the dynamical behavior of such multi-arm robotic devices and the influence of the vibrations on the accuracy of the device.

PROJECT LEADER:	Dr. Szilágyi Attila *associate professor*
CONSULTANT:	Thomas Alves da Silva Wallyson *PhD student*
RELEASE DATE:	10th February, 2021.
SUBMISSION DATE:	30th April, 2021

MISKOLCI EGYETEM * Gépészmérnöki és Informatikai Kar * Szerszámgépészeti és Mechatronikai Intézet * 2.

....

Dr. Szilágyi Attila associate professor
Head of Institute

1. Modification of thesis: *necessary (modificitaion on a seperate sheet)*
not necessary

Miskolc, ……………………………….. ……………………………
project leader

2. Check dates:

…………………………	…………………………
…………………………	…………………………
…………………………	…………………………
…………………………	…………………………

3. The thesis is *submissible*
not submissible

Comments: ………………………………………………………………………………………………………

………

Miskolc, …………….. …………………. ………………….
consultant *project leader*

4. The thesis contains .... *written pages,*
.... *drawings,*
.... *other appendices,*
.... *CD appendices.*

5. The thesis *can* *be reviewed.*
can not

Name of reviewer: ....

Miskolc, ……………………………….. ……………………………
Dr. Attila Szilagyi
head of department, associate professor

6. Grade:

suggestion of reviewer: ……………………………………………………………….

suggestion of department: ……………………………………………………………….

decision of the Final Examination Committee: ……………………………………………………………….

Miskolc, ……………………………………

....
chairman of Final Examination Committee

Acknowledgements

I wish to express my sincere gratitude to my supervisor, Dr. Szilágyi Attila for his guidance during the development of this research. I will also like to thank Wallyson Thomas and Alzghoul Mohammad for their invaluable support and feedback which contributed imensely to the success of this work. In addition, I would like to thank my colleagues and members of the Institutional Department of Machine Tools, University of Miskolc for their contributions. Finally, I wish to express my profound gratitude to my family and friends for their continous love, support and encouragement.

Miskolc, 30th April 2021

FELIX Bernard

Contents

List of Figures

List of Tables

Abbreviations

BC	Boundary Condition(s)
CAD	Computer-Aided Design
CAE	Computer-Aided Engineering
D-H	Denavit-Hartenberg
DoF	Degree(s) of Freedom
EE	End-Effector
EOM	Equation(s) of Motion
FEA	Finite Element Analysis
FEM	Finite Element Method
FK	Forward Kinematics
IK	Inverse Kinematics
MDoF	Multi-Degree of Freedom
MBS	Multi-Body System
PDE	Partial Differential Equation(s)

Abstract

Designing an industrial robotic structure is known to be a complex endeavor owing to the different product specifications which must be met, while taking several constraints of the system's structure such as weight limitations into consideration. In this work, an in-depth design approach is presented whereby theories of the mechanics of serial-linked robotic structures were critically investigated in order to adopt and present a concise analytical and computer-aided approach to the design of a 6-DOF industrial robotic structure.

The CAE tools have come to make the job of design engineers incredibly easier, however, beyond just using these tools to obtain information about the system, it is necessary to setup a sufficiently representative mathematical model of the numerically simulated systems for verification purposes. Furthermore, by setting up and evaluating an analytical model, the engineer can easily vary the geometrical and natural parameters as well as the constraints within the system's model in order to achieve an optimized structure according to the design expectation. One of such design requirements is attaining a sufficient stiffness of the robotic structure, within weight constraints in order to guard it from vibrations which could negatively impact its operational accuracy.

In order to practically demonstrate this concept, numerical finite element analysis and mathematical modelling of the vibrations that could occur on the designed industrial robot's link arm are presented in this study. The analytical procedure which is presented in this thesis report can be applied to both simplified robot model design, analysis and verification, and it can also be adopted or serve as a basis for the design of a more complex robotic system than the one presented in this study.

1 Introduction

The *Finite Element Method* (FEM), which was first developed as a procedure for static structural analysis has gained an immense amount of popularity as an engineering analysis tool with extension to cater for vibration and fluid analysis, etc. When integrated into a *Computer-Aided Engineering* (CAE) design process, the basis for which lays in kinematic simulation, dynamic simulation and structural analysis, FEM has helped engineers to save considerable amount of time and financial resources while delivering immense productivity and cutting-edge innovation in robotics design.

The field of robotics has experienced tremendous developments within the past decades and is identified as one of the key elements of Industry 4.0; the fourth industrial revolution [1],[2]. This is one of the key areas where mechanical design goes beyond the traditional design, analysis, optimization and development of mechanisms and mechanical systems, but is fully integrated with more robustness by incorporating electronic and computer-based manipulation and control capabilities, and in some instances artificial intelligence. For any mechanical design engineer who is seeking holistic and innovative product design competencies which are both relevant for present and future applications, it is a worthwhile endeavor to acquire knowledge of robotics and/or automation technology, and even more beneficial to acquire essential mechanical design background within robotics and automation systems.

1.1 Problem Definition

The design of robotic structures is mostly complex owing largely to design considerations for robot's dynamic properties such as its accuracy, repeatability, stability and compliance which have to be duly considered during the design process. Engineers and designers in the robotics industry have come to heavily rely on CAE techniques to better understand these highly complex physical design problems by creating virtual CAD models and simulating them with commercial and FEM codes to obtain computed numerical results and graphical representations which can provide useful information about their design. Hence, design ideas can be readily tested without having to spend money or invest effort in building models. With this, faulty areas can be discovered within proposed design, design modification ideas can be simulated, and designs can be quantized and optimized; bearing in mind the required dynamic characteristics of the specific robot design.

A common practice in using simulation tools for CAE is the case of fully depending on the results provided by these simulation tools, without verifying or validating them. This is due to the fact that doing these usually requires a deep understanding of the physical problem and how to mathematically model them, after which complex analytical techniques are usually required to solve the mathematical problems. Vibration of robotic manipulator structures is the major limitation of robotic operational capacities, especially for high precision tasks. During machining for instance, if low frequency modes are present in the system, the entire body of the robot will be shaken as it vibrates, leading to instability of the robotic structure. Various loading conditions on the robot are also capable of causing plastic deformations on its links that may lead to dynamical inaccuracies over time. In order to make the appropriate decisions after obtaining simulation results regarding the robot's structure and dynamic behavior, it is important to be able to know how the simulation tool came about those results. By being able to compare numerical results against analytical solutions, more accurate decisions can be made.

In this study, a replica of the KUKA KR 15/2 industrial robot's main body by KUKA robotics has been designed and structurally investigated. Ever since the original design of the robot approximately twenty (20) years ago, there has been significant developments in both the software and hardware tools used for CAE implementation. The FEM codes have been developed to have better computational capabilities and the graphic interface within modern software also offers much more flexibility to the design engineer with lots of sophisticated features. Some CAD software are now even integrated with simulation tools to offer an integrated CAE modelling environment. The hardware as well has developed immensely, having been equipped with better processors to handle the additional sophistication of the FEA tools at relatively faster speed. It is therefore expected that with the use of the features in modern CAE tools, a more accurate dynamic and structural investigation of the attributes of the robot can be carried out. Specifically, it will be investigated that the structure of the replica industrial robot in this study has an excellent structural integrity and frequency spectrum, and that it complies to the original design attributes or specifications such as cost-effectiveness, lightweight construction and high torsional and flexural rigidity [3].

1.2 Aim and Scope

In a bid to provide objective guidance for taking important error-mitigating, failure-preventing and cost-saving design decisions, this thesis work primarily aims at practically exploring the utilization of CAE within the field of robotics mechanical design to investigate the dynamical characteristics of modern CNC robotic machining centers and verification of the results of some of those numerical investigations through analytical hand computations. Bearing the design objectives in mind, this thesis work has been carried out in three main stages of preliminary design, verification computations and numerical analysis.

At first, a replica of KUKA KR 15/2 industrial robot structure was optimally designed, having the capacity to carry out the same family of tasks and having a similar workspace, maximum reach and loading capacity. This means that both robots have a closely similar topology which largely influenced decisions about the geometric features and dimensions of the robots' links and joints. Similar to the KUKA KR 15/2, the main bodies of the moving principal assemblies of the replica robot are expected to be manufactured of cast light alloy and it is expected to be characterized by good dynamic performance with high resistance to vibration as a result of the structure having a high natural frequency [3]. The focus of the activities in the ensuing design stages will be to ensure that these optimal design requirements are duly met.

The verification stage involved carrying out *hand computations* with which to obtain some approximate analytical results for vibrations in the robotic system. These results served as predictions, used to verify the numerical simulation results which were obtained from the FEA tool at the later stage of the work. This process also helped with exploring major elements that make up the simulation tool (commonly referred to as *The Blackbox*). As it will be seen in later sections of this report, the process involves definition of the mathematical model which includes the governing equation of motion, the underlying physical principles, boundary conditions and assumptions which are commonly used in frequency simulations. Attention has also been drawn to the use of FEM as an approximate computational technique adopted to analytically solve the mathematical model of the vibrating system (the eigenvalue problem).

At the third and final stage, commercial CAD and FEM code was leveraged to model the solid structure of the designed robot and to compute its mechanical behavior with static stress analysis and modal analysis. The aim here was to check the performance of the design and to investigate the system's compliance to original design specifications such as the stability and rigidity of its structure, hence drawing conclusions on its suitability for industrial applications. Checks were carried out for the robot's capacity to resist vibrations and plastic deformations that are large enough to negatively impact its dynamic performance during operation. The following investigations were carried out under two highly demanding configurations of the robot:

a. Solid modelling of the designed robot with CAD tool within an integrated CAE design software,
b. Static structural analysis of the entire robot structure by means of FEA tool,
c. Modal analysis of the entire robot model,
d. Modal analysis of the robot's link arm.

The numerical analysis results were compared against the analytical mathematical modelling results in order draw conclusions on the structural and dynamical behavior of the system and how these will impact on the dynamic properties during operation, such as its accuracy and stability. These results were also useful to confirm the claims of the preliminary design, as well as to identify room for possible optimization or compromises to make on the preliminary robot design to ensure that it more suitably satisfies the laid-out design objectives.

1.3 Research Questions

To aid the success of this work, research questions were formulated to guide and structure the study, which were answered at the end of each stage of the study. The first question addresses background knowledge on robotic structural mechanics and FEA, whereas the remaining questions focus on the actual study. The research questions were as follows:

I. Are the maximum resultant stresses and displacements experienced by the simulated robotic structure under the prescribed loading condition all below the material yield stress and within the allowable deformation limits?
II. Are the numerical results obtained from the frequency analysis consistent with the system's mathematical model; and do they have a reasonable comparison?
III. Are the vibrations experienced by the robot within acceptable limits, and does it have permissible influence on the robot's dynamic accuracy upon experiencing different kinds of loading during operation?
IV. Does the design meet all design objectives?
V. Bearing the design objectives in mind, as well as the results drawn from this study, is there room for modification of the robot's structure to achieve a more optimized design?

1.4 Thesis Report Layout

The report begins with a literature review in Chapter 2, where the reader will find background knowledge and references on industrial robots, their classifications and applications. Furthermore, this chapter elaborates on industrial robots' key attributes which are relevant to this study. The main issues in robot design are also addressed in this chapter, with a section dedicated to description of the mechanical structure of serial-link industrial robots. The final section of this chapter reviews the state-of-the-art in the application of CAE to the design and analysis of complex robotic structures. In Chapter 3 the essential technical specifications for the robot designed in this study are laid out. Chapter 4 contains sequentially, all the design activities that were carried out in order to arrive at a robot design which was ready for CAD modelling and analysis, including kinematic, dynamic and elastostatic design. The CAD model of the robot is presented in Chapter 5, as well as the several analyses that were carried out on it, including a proposed analytical technique for verification of the numerical results of vibrations which are experienced by one of the robot's links. To round up the work, concluding remarks about the robot's design can be found in the sections that follow Chapter 5, as well as recommendations for future study involving the complete industrial robot design.

2 Literature Review

In this part of the report, a general introduction to industrial robots is presented, as well as information on some relevant previous research studies on robotic manipulator design and dynamic characteristics identification, all of which were keenly studied during the course of this thesis work. The studies include approaches with which to tackle critical design problems in the field of robot design such as robot dynamics and mechanism design; kinematic calibration and accuracy measurement of industrial robotic manipulators; and integrated computer-aided engineering as it relates to industrial robot design, where structural and dynamic analyses are implemented. Some of the study results presented involved pure theoretical investigations; others involved analysis with computational tools and experimental verification, while some involved a combination of several of these approaches.

2.1 Industrial Robots

In light of the advent of Industry 4.0 which has factory automation as one of its primary components, industrial robots have steadily come to find a permanent place in the production floor of most large and mid-sized manufacturers, such as those in the automotive industry. The first company to manufacture these special mechanical structures was F. Euglelberger in 1956, which produced the 'Unimation' robot. Unimation robots were based on an original patent filled by George Devol in 1954 as the first patents in robotics. These robot's axes were actuated hydraulically and they were used primarily for pick-and-place applications.

With steady development of the technologies that power them, these mechatronic systems have advanced rapidly into an important provider of versatility to manufacturers due to their ability to be reprogrammed for various purposes. One industrial robot can be reprogrammed to have multiple use-cases such as in spot welding, manufactured parts assembly, machining, spray painting, and on production lines for material handling operations, etc. These robots come in varieties of designs; some are designed such that they can be fixed at a specific location or job post, while some are equipped with mobility capabilities. However, a common theme in the design of industrial robots is their anthropomorphic and serial-linked structure.

2.1.1 General Features of Industrial Robots

With exception to gantry and parallel-linked types, most industrial robotic manipulators or *‘arms’* as they are commonly called, obtain their name from their anthropomorphic structure. These robots are usually designed to have an open-chain, serial-linked structure. When compared to the anatomy of humans, their links can be likened to the chest, upper arm, and forearm, while their joints can also be referred to as to the shoulder, elbow and wrist of the robot. The industrial robot’s structure can only move, but on its own is not capable of carrying out any tasks. To give it actual functionality as a production or manufacturing system, the end of the arm’s structure is usually equipped with an end-effector (EE), which is also called end-of-arm tool, gripper, or hand. The tool often has two or more fingers that open and close, but different kinds of tooling can be attached to the robot. Depending on what specialized function the robot has been programmed to perform within a production facility, grippers, holders, and various other specialized tools can serve as end-effectors.

2.2 The Mechanics of Robot Design

A critical issue to consider when first embarking on a robot design has to do with choosing the geometry of the robot’s workspace, which is largely dependent on the family of tasks which it should be capable of performing and the working environment where it is intended to be used. Other critical aspects which the robotic design engineer has to deal with include evaluating and deciding on the *kinetostatic*, *dynamic*, *elastostatic* and *elastodynamic* performances of the robot [4]. To support static loads which are assumed at the outset of a serial-link robot design process, their links and joints are structurally dimensioned during the kinetostatic design process, which is determined by the workspace requirements of the robot and its topology. In order to determine the required motor torques which can drive the robot’s axes, the centers of mass of the robot’s links and their inertia matrices are evaluated during the dynamic design phase. Since the evaluation which is carried out does not take the motors significant dynamic loads at the robot’s joints into consideration, it is regarded as only a preliminary design phase. For elastodynamic modelling, rigid links and stiff joints are usually assumed, and new analysis is usually required after actuator selection in order to incorporate the structural and inertial data of the chosen actuators.

Hence, robotic motion design study can be broadly categorized into two areas of ***kinematic design*** and ***dynamic design*** [5]. Furthermore, the structural behaviors of the links and joints are investigated during ***elastostatic design,*** including vibrations to ensure that robot's links and joints will be able to counter the possible resulting deflection which could arise as a result of loading while in operation. And lastly, during ***elastodynamic design*** the system is analyzed as though it were to be in operation and moving, so as to achieve optimal dynamical operating characteristics for the robot. A short review of the mathematics behind each of these studies will be briefly outlined in the ensuing sections of this chapter.

2.3 Challenges in Industrial Robot Design

Many industrial robot manufacturers such as KUKA Robotics, develop specialized components and end-of-arm tools with which their robots can be deployed as CNC machining centers for milling operations [6]. The major advantage of using robots for such high-precision-demanding tasks over traditional machines is their movement flexibility, high endurance, consistency, speed, and of course, precision capability. However, recurring theme in industrial robots' application in industry has been with being able to get them to perform their tasks efficiently; an aspect which concerns their dynamic characterization and capabilities. For instance, a robotic milling machining center can only produce high quality products if it is capable of precisely maintaining a high positioning accuracy throughout the duration of its operation.

This, therefore has been an aspect of concern for industrial robot designers and has also led to an expansive area of academic research concerned with finding solutions to robot dynamical efficiency problems such as operational accuracy. The tolerance level to which an industrial robot must be designed to satisfy dynamic properties depends on the purpose for which it is designed, and this determines the type of tooling which should be attached to its end-effector [7]. Compared to tasks such as spray painting, robots used as CNC machining centers, strictly require stability of its structure during operation; the robot should also have high repeatability capacity; and very essential is the requirement for its accuracy level to be excellent.

Calibration of the industrial robots is one practice which has become common for identifying errors in the accuracy and repeatability of robots and compensating them. Errors arising from the geometry of the robot as well as its kinematic design are some of the major contributors to inaccuracies in robots [8]. These issues typically arise as a result of links and joints deflections in the robot, hence by designing stiffer mechanical robotic structures, it can be ensured that the geometric and kinematic errors which the calibration systems will have to identify in order to be compensated for will be very minimal. This is the focus of this present study.

2.3.1 Dynamical Properties Identification

Deviations in dynamical parameters of the robot such as its accuracy and repeatability mean that the robot is unable to decipher where it is precisely. A robot with repeatability issues will be unable to repeatedly orient its end-effector in the same position when required to. Inaccuracies on the other hand, refer to the inability for the robot to orient itself in an arbitrary position only when commanded to, without returning to that pose when it is not required to. For robotic CNC machining centers these properties are very critical since for such application, the position of the robot's end-effector and the trajectories which it follows during the machining task are usually not being computed by the robot controller itself.

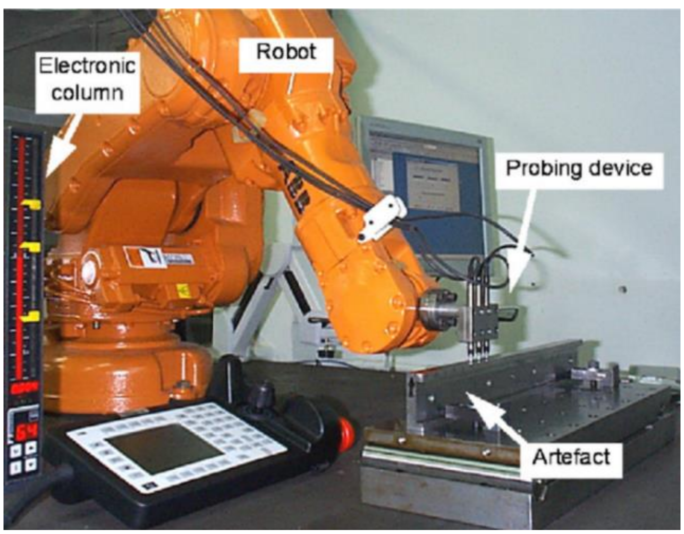

Figure 2. 2: *Automated measuring system attached to an industrial robot [10].*

For the sake of precision in robots used for machining operations, as well as for assembly robots, it is always advisable to ensure that the current dynamical state of an industrial robot is sufficient for the intended task before putting the system to use. For this purpose, calibration and accuracy measurements of the robot has become a common practice. For robotic assembly applications for instance, robots having greater than $0.1mm$ positioning error are not suitable for use, and a proposed means for obtaining a sufficiently precise data for such measurement involves the use of automated laser interferometer system, which can be seen illustrated in figure 2.1 [9],[10].

The effectiveness of robotic accuracy compensation techniques such as this can be verified analytically through hand computations in order to find out the primary source of the errors identified by the calibration experiment. This necessitates investigations regarding the theoretical background of robot mechanical design which is presented in the next section.

2.3.1.1 Robot Kinematical Modelling

Kinematics investigates the connection between motion properties such as the position and velocity of objects without consideration of the forces and moments that create the motion. In robotic systems, collision prevention, singularity elimination, and system redundancy are some of the factors which their kinematic design can deal with [11]. It can be applied to determine the end-effector's velocity and acceleration; its reach, and oriented rotation while designing and analyzing the robotic system. The study of the geometric relations between *joint* and *Cartesian variables* of a serial-linked robotic manipulator structure is where its kinematic design begins [5]. Joint variables of a given manipulator determine its posture. With each joint having such variable, typical industrial robotic manipulators which are serial-linked and have six-axes therefore have six joint variables which are denoted in this study by: q_1, q_2, q_3, q_4, q_5 and q_6. On the other hand, these manipulators also involve six Cartesian variables which define the pose (position and orientation) of their end-effector. A combination of position (x, y and z) and orientation (roll, pitch and yaw angles) can be used to define the end-effector's pose.

$$\xi_E \sim (x, y, z, \theta_r, \theta_p, \theta_y) \tag{2.1}$$

In modelling the geometry and kinematics of robotic manipulators, two problems are defined, namely direct kinematics and inverse kinematics. *Direct* or *forward kinematics (FK)* motion study considers the situation in which the associated connecting joint variables and geometric link parameters of the manipulator are assumed to be known, while the problem consists in finding the end-effector location or pose, rotation, speed, and accelerated rate with respect to a reference coordinate frame. *Inverse kinematics (IK)* motion study considers the situation in which the end-effector position or pose values are given, while the six connecting joint values or variables that produce this pose are to be computed.

2.3.1.1.1 Forward Kinematics

To aid in describing their kinematics, the D-H notation is a general way for describing the structure of complex serial-link manipulator mechanisms. The notation is named after Jacques Denavit and Richard Hartenberg who in 1955 proposed a consistent and concise method to deal with kinematics of open serial chains, known as D-H parameters method [12]. The pose of the robot's end-effector, which is considered as the direct kinematics problem can be fully defined by successive multiplication of the D-H homogeneous transformation matrices between its links, from the base of the manipulator towards its end- effector [13].

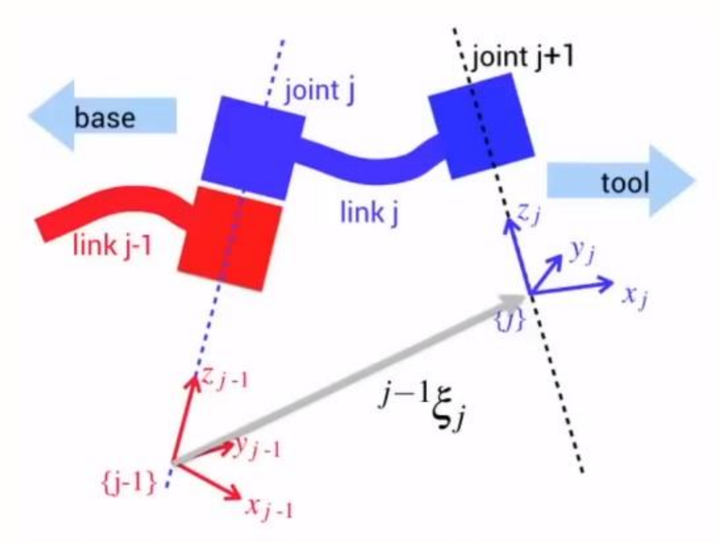

Figure 2. 3: *Representation of two serial robot links with reference frames attached [14].*

With reference to figure 2.2, the D-H notation is implemented by attaching a coordinate frame to the far end of each link in the robot, and then, writing an expression for the relative pose between consecutive link reference frames with respect to the link coordinate frame of the joint [14].

The D-H parameters also find use in dynamical properties identification and compensation techniques which involve kinematic calibration as presented in [15]. There are exactly one joint variable and three constant parameters associated with each joint of a robot. Hence, a 6-axis manipulator has six (6) joint variables and eighteen (18) constant parameters [5]. For this current study, a D-H notation table which describes the structure of the industrial robotic manipulator's mechanism has been formulated and is presented in table 4.1.

2.3.1.1.2 Inverse Kinematics

The inverse kinematics of a robot deals with the computation of its joint angles given its end-effector's desired position and orientation and information about the geometric link parameters of the manipulator. This problem is more challenging and has been researched at length, leading to both analytical and numerical techniques for its evaluation. The inverse kinematics equations for the angles of a six (6) DoF robot was summarized in [10].

2.3.1.2 Robotic Motion in 3D (Velocity Kinematics)

To aid with accuracy investigations, the Jacobian matrix can be used in the analysis of the positioning error in industrial robots [16]. The Jacobian matrix symbolizes velocity kinematics, which describes the relationship between the robot's joint velocities and its end-effector. Instantaneously, the velocity of the end-effector is the sum of its velocity components due to the motion of each individual joint. Furthermore, it will be seen in section 2.3.3 that this very important matrix also finds use in vibrational modelling of serial robotic manipulators as it helps to map the system's stiffness matrix in the joint space, $\mathbf{K}_q$ to same in the Cartesian space $\mathbf{K}_c$ in order to conveniently compute the matrix's eigenvalues. In this study, velocities of the robot's joints are represented by $\dot{q}_i$, while $\dot{\xi}$ represents the rate of change of the end-effector's pose. The instantaneous velocity of a robot's end-effector in 3-dimensions can be described by a single six-element vector called the spatial velocity or twist of the robot's end-effector, which in this case is comprised of six (6) parameters as shown below.

$$v = \left(\dot{x}, \dot{y}, \dot{z}, \omega_x, \omega_y, \omega_z\right)^T \tag{2.2}$$

The spatial velocity comprises of two velocity components; the translational and angular velocity components, which change continually as the object is moving and have three (3) components each. A 6-axes industrial robot will have a 6×6 Jacobian matrix, and its elements express the rate of change of the robot's end-effector coordinates with respect to its joint coordinates [17]. The linear relationship between joint angle velocity and end-effector velocity is given by equation 2.3.

$$v = \boldsymbol{J}(q)\dot{\boldsymbol{q}} \tag{2.3}$$

It is common in practical applications to desire a particular end-effector velocity for the robot. By computing the Jacobian and inverting it, the velocity of the joint angles that is needed in order to achieve that desired end-effector velocity can be obtained. The Jacobian matrix is a matrix which when inverted will result in the expression in equation 2.4. This is useful when it is desired for the robot's end-effector to move in a particular velocity without having to compute its inverse kinematics.

$$\dot{\boldsymbol{q}} = \boldsymbol{J}(q)^{-1} v \tag{2.4}$$

2.3.2 Robot Dynamics Modelling

After carrying out the kinematics design to obtain associated locations, speeds, and accelerations, dynamics modelling is required in order to determine the effect of forces on the robot structure's motion [11]. Dynamics can be classified into forward or direct dynamics and inverse dynamics. Forward dynamics is concerned with figuring out how a robot will move when certain forces are applied to the robot or torques are applied at the actuators of the robot. Inverse dynamics on the other hand, has to do with figuring out the driving forces, torques or motor currents required for a robot to move or accelerate in a particular way; this is used in solving robot control problems.

2.3.2.1 Inverse Dynamics

To model the dynamics of the 6-link robot, the Lagrangian approach can be used which requires the generation of Lagrange's equations of motion. The Lagrangian approach requires expressions for kinetic and potential energy, and external force and moments; hence unlike Newton-Euler method, deriving explicit expressions for accelerations is not necessary. The Lagrangian approach offers engineers certain advantages in the computation of dynamics for complex systems such as robots with multiple links since it requires only position analysis and velocity analysis. The Lagrangian is defined as the difference between the kinetic energy of a system and its potential energy.

$$\mathcal{L}(q, \dot{q}) = \mathrm{K}(q, \dot{q}) - \mathrm{P}(q) \tag{2.6}$$

$$\frac{d}{dt}\left(\frac{\partial \mathcal{L}}{\partial \dot{q}}\right) - \frac{\partial \mathcal{L}}{\partial q} = \tau \tag{2.7}$$

If any of the forces has potential, the Lagrangian can be written in this general form:

$$\frac{d}{dt}\left(\frac{\partial \mathrm{K}}{\partial \dot{q}_l}\right) - \frac{\partial \mathrm{K}}{\partial q_l} + \frac{\partial \mathrm{P}}{\partial q_l} = \tau_l \tag{2.8}$$

Equation 2.7 or 2.8 is called the *Euler-Lagrange Equation*. In general, the Lagrangian is a function of the position $\boldsymbol{q}$, the velocity $\dot{\boldsymbol{q}}$. The potential energy will only be a function of $\boldsymbol{q}$. A 6-link robot is a 6-order system since it requires six (6) generalized coordinates to describe its motion. For a 6-link rigid robot, the set of generalized coordinates is represented by its six (6) D-H joint variables [17]. The inverse dynamics of a serial-linked robotic manipulator, which is described by the general Euler-Lagrange EoM can be expressed concisely in matrix form as shown in equation 2.9. This inverse-dynamics function maps the displacement, velocity and acceleration of the robot ($\boldsymbol{q}, \dot{\boldsymbol{q}}, \ddot{\boldsymbol{q}}$), to the torque applied at the robot's joints.

$$\mathbf{M}(\boldsymbol{q})\ddot{\boldsymbol{q}} + \boldsymbol{C}(\boldsymbol{q}, \dot{\boldsymbol{q}})\dot{\boldsymbol{q}} + g(\boldsymbol{q}) = \boldsymbol{\tau}(t) \tag{2.9}$$

The Greek letter $\boldsymbol{\tau}$ represents vector of torques which are applied at the robot's joints; $\mathbf{M}(\boldsymbol{q})$ is the inertia matrix (or $n \times n$ mass matrix) of the manipulator; $\boldsymbol{C}(\boldsymbol{q}, \dot{\boldsymbol{q}})$ which depends on both position and velocity, is an $n \times 1$ vector which includes what are known as the Coriolis and centripetal terms; $g(\boldsymbol{q})$ which is dependent on only joint coordinates is the torque which arises from gravity acting on the robot's structure.

Frictional forces are non-rigid body effects which the manipulator experiences at its joints. In present-day manipulators, these forces can equal as much as 25% of the torque required to move the manipulator in typical situations [18]. These forces can be modelled into the dynamic equations by including viscous and Coulomb friction models in order for it to reflect the reality of the physical system. The new equations of motion can be expressed in matrix form as shown in equation 2.10, where $\tau_f = f(\boldsymbol{q}, \dot{\boldsymbol{q}})$ represents the friction model introduced into the system.

$$\mathbf{M}(\boldsymbol{q})\ddot{\boldsymbol{q}} + C(\boldsymbol{q}, \dot{\boldsymbol{q}})\dot{\boldsymbol{q}} + g(\boldsymbol{q}) + \boldsymbol{f}(\boldsymbol{q}, \dot{\boldsymbol{q}}) = \tau(t) \tag{2.10}$$

In order to practically compute the six (6) equations of motion required for the 6-order system, the potential and kinetic energies of the system should be computed with the equations 2.11 and 2.12, respectively.

$$\mathrm{P} = \sum_{i=1}^{6} P_6 = \sum_{i=1}^{6} \boldsymbol{g}^T \boldsymbol{r}_{c_i} m_i \tag{2.11}$$

$$. \mathrm{K} = \sum_{i=1}^{n} \left(\frac{1}{2} m \boldsymbol{v}_{c_i}^T \boldsymbol{v}_{c_i} + \frac{1}{2} \boldsymbol{w}_{c_i}^T \mathbf{I}_i \boldsymbol{w}_{c_i} \right) \tag{2.12}$$

In rigid body dynamics, gravity is the only source of potential energy. In the potential energy expression of equation 2.11, $\boldsymbol{g}$ is the vector which gives the direction of gravity in the inertial frame, while $\boldsymbol{r}_{c_i}$ gives the coordinates of the center of mass of link i. The linear and angular velocity terms, $\boldsymbol{v}_{\boldsymbol{c}_i}$ and $\boldsymbol{w}_{\boldsymbol{c}_i}$in the kinetic energy equation, is usually expressed in terms of the position vectors of the center of mass of each of the links of the robot and their associated velocities. However, with the Jacobian which was earlier discussed, the kinetic energy can be re-expressed in terms of generalized coordinates rather than workspace coordinates, where m is the mass of each of the links of the robot, and I, the inertia matrix of each of the links, which is evaluated around a coordinate frame parallel to the link in consideration. This is more useful since to compute the Lagrangian all the components of the equation must be expressed in terms of the generalized coordinates.

$$\mathrm{K} = \frac{1}{2}\dot{q}^T \sum_{i=1}^{6}\left[m_i \boldsymbol{J}_{\boldsymbol{v}_{c_i}}(\boldsymbol{q})^T \boldsymbol{J}_{\boldsymbol{v}_{c_i}}(\boldsymbol{q}) + \boldsymbol{J}_{\boldsymbol{w}_{c_i}}(\boldsymbol{q})^T R_i(\boldsymbol{q}) I_i R_i(\boldsymbol{q})^T \boldsymbol{J}_{\boldsymbol{w}_{c_i}}(\boldsymbol{q})\right]\dot{\boldsymbol{q}} \tag{2.13}$$

The inertia tensor in equation 2.13 is a 3×3 symmetric matrix which can be computed explicitly as follows:

$$I = \begin{bmatrix} I_{xx} & I_{xy} & I_{xz} \\ I_{yx} & I_{yy} & I_{yz} \\ I_{zx} & I_{yz} & I_{yy} \end{bmatrix} \tag{2.14}$$

2.3.2.2 Forward Dynamics

Forward dynamics is used to dynamically simulate robot motion with a controller. With knowledge of the torques and forces that should be applied to the robot manipulator, the motion of the robot (q, $\dot{q}$. $\ddot{q}$), can be computed as a function of time. Equation 2.10 can be rearranged to obtain an expression for joint acceleration, $\ddot{q}$ in terms of the torque that is applied to the robot, and this expression when integrated with respect to time will yield an expression for joint velocity, $\dot{q}$. By integrating again, an expression for the joint position, $\boldsymbol{q}$ is obtained.

$$\ddot{\boldsymbol{q}} = \mathrm{M}^{-1}(\boldsymbol{q})\{\tau - C(\boldsymbol{q},\dot{\boldsymbol{q}})\dot{\boldsymbol{q}} - g(\boldsymbol{q}) - f(\boldsymbol{q},\dot{\boldsymbol{q}})\} \tag{2.15}$$

$$\dot{\boldsymbol{q}} = \int \ddot{\boldsymbol{q}}\, dt \tag{2.16}$$

$$\boldsymbol{q} = \int \dot{\boldsymbol{q}}\, dt \tag{2.17}$$

These set of equations define the forward dynamics function, which gives the motion of the robot as a function of the torque applied on the robot.

2.3.3 Vibrations in Industrial Robots

Excellent dynamic characteristics are expected of industrial robotic manipulators, such as its accuracy, repeatability, stability and compliance all of which become even more critical design issues to deal with when the robot is required to be used as a CNC machining center. Due to the design requirement to lower the weight of industrial robots as much as possible, one of the common causes of vibrations in robotic structures is the lack of sufficient stiffness in its links, which results in deflections. Joint deflections, which is another aspect of robot design to look into when considering vibrations, was experimentally identified by modal analysis in [19].

These deflections, when large enough can lead to total failure of the system. However minimal vibrations as a result of minor deflections in different parts of the robot are still important to eliminate from the design as much as possible, as they can lead to a considerable shift of the robot’s end effector away from its ideal position during operation. This is regarded as positioning error, and it can affect the dynamic properties of the robot such as repeatability and accuracy, negatively. For optimal robot design, a quick way to deal with this problem is by making the robot’s links extremely rigid, however, by using increasingly stiff materials such as steel for their manufacture, the weight of the links increases, thereby requiring more powerful electric motors with higher torque rating for their actuation.

2.3.3.1 Elastostatic Modelling

The assumption of rigid links in the EoM earlier presented means that deflections were not taken into consideration. In a state of static equilibrium, to understand the robotic structure’s response to real applied load will require obtaining its elastostatic model, which may be measured in terms of the structure's stiffness. When the robot's end-effector is subjected to an applied wrench, different parts of the structure will respond according to its stiffness with a certain amount of translational and angular deflection [4]. Depending on the objectives and on the nature of the system's parameters, the same vibrating system can be mathematically modelled as a *discrete (lumped-parameter) system* or *continuous (distributed-parameter) system* to obtain similar vibrational characteristics, and some literatures on the subject were reviewed in order to better understand these modelling cases and their relevance to analytic vibration analysis in the field of robotics.

2.3.3.1.1 Discrete Modelling of Joint Deflections

Vibrating systems like industrial robots are typically comprised of an assembly of individual components acting together as a whole, but by adopting a discrete modelling approach the components of the serial robot system can be discretized, with the system parameters (mass and stiffness in this case) comprising of the masses of the robot's link's which are assumed to be rigid and concentrated at individual points; and stiffness of linearly elastic and massless torsional springs which the robot's joints were assumed to be made of, thus serving as connectors for the rigid masses. As a result of such modelling approach, the number of distinct natural frequencies and their corresponding natural frequencies of vibration obtained will depend on the DoF of the system.

In order to embark on vibration analysis of any system, it is paramount to first establish the governing equation(s) of motion for the system. For a lumped-parameter system, these are second-order ordinary differential equations, and their number depends on the number of the system's degrees of freedom, which in itself is generally defined by the number of masses that the system is discretized into. Hence, there is one ordinary differential equation which governs the motion of each mass in a lumped-parameter system, and these are usually coupled together to obtain the complete governing equation of motion of an n-DoF. An advantage of discrete modelling is that it is relatively easier to compute the response of a discrete system to a specified excitation since the solution of a set of coupled ordinary differential equations is easier to obtain than partial differential equations which are involved in continuous modelling. Before the governing equations of motion can be generated for the system, it is necessary to identify the system's components and to establish the characteristic response of those components to excitations. In broad terms, these components comprise of springs with forces proportional to the system's displacements; dampers with forces proportional to system velocities; and finally, masses with forces proportional to the system's accelerations.

A method for analyzing serial-link robot's elastostatic performance is proposed in [4]. The author is concerned with the deflections that occur at the robot's joints, hence the objective for the elastostatical modelling was to achieve a minimum permissible value for the possible maximum deflection that the robot could experience at its joints [4]. Equation 2.18 defines the linear relationship between vector $\delta\boldsymbol{q}$ of variations in the joint angles and vector $\boldsymbol{\delta\tau}$ of elastic joint torques, both of which are 6-dimensional for a 6-link robot.

$$\boldsymbol{\delta\tau} = \mathbf{K}_q \delta\boldsymbol{q} \tag{2.18}$$

Where, at the specified posture of the robot, $\mathbf{K}_q$ is the system's *n* x *n* positive-definite *stiffness matrix* which is defined in joint space; $\delta\boldsymbol{q}$ is joint-variable elastic displacements and $\boldsymbol{\delta\tau}$ is the perturbation torque which the robot's elastic joints are subjected to when they are locked. $\mathbf{K}_q$ is the diagonal matrix presented in equation 2.19, and its elements represent the robot's joints torsional stiffnesses at that posture.

For a 6-link robot:

$$\mathbf{K}_q = \begin{bmatrix} k_{q_1} & 0 & 0 & 0 & 0 & 0 \\ 0 & k_{q_2} & 0 & 0 & 0 & 0 \\ 0 & 0 & k_{q_3} & 0 & 0 & 0 \\ 0 & 0 & 0 & k_{q_4} & 0 & 0 \\ 0 & 0 & 0 & 0 & k_{q_5} & 0 \\ 0 & 0 & 0 & 0 & 0 & k_{q_6} \end{bmatrix} \tag{2.19}$$

The deflection in the robotic system can be obtained from computing the eigenvalues of the system's stiffness matrix $\mathbf{K}_q$, or its inverse, $\mathbf{C}_q$ (compliance matrix). Thus, achieving the objective of elastostatical modeling is related to the stiffness constants in the stiffness matrix. For a constant change in elastic joint torque $\delta\boldsymbol{\tau}$, the eigenvector direction, which relates with the stiffness matrix's minimum eigenvalue, k_{min} or with the maximum eigenvalue of its inverse c_{max}, will yield the maximum deflection. The higher the natural frequency, the higher the stiffness (lower deflection), and maximum eigenvalue yields maximum natural frequency, and vice-versa. To minimize the maximum deflection that could occur in the system, the minimum eigenvalue of the stiffness matrix needs to have a value that is as high as possible, i.e., it should be as close to k_{max} as possible (higher stiffness constants, will result in lower deflections). To enable the analysis of the elastostatic properties of a serial robotic manipulator in joint space by solving for its eigenvalues, the magnitude of the stiffness constants can be evaluated by taking the weighted Frobenius norm of the stiffness matrix $\mathbf{K}_q$ [5].

The elastostatic properties of a serial robotic manipulator can also be defined in the Cartesian space in terms of the Cartesian stiffness matrix $\mathbf{K}_c$, with the relation in equation 2.20 [20]. A comparison between equations 2.18 and 2.20 will result in the relationship that exists between $\mathbf{K}_q$ which defines the stiffness matrix in joint space, and that of the Cartesian space, $\mathbf{K}_c$.

$$\delta\boldsymbol{\tau} = J^T \mathbf{K}_C J \delta\boldsymbol{q} \tag{2.20}$$

$$\mathbf{K}_q = J^T \mathbf{K}_c J \tag{2.21}$$

$$\mathbf{K}_c = J^{-T} \mathbf{K}_q J^{-1} \tag{2.22}$$

Where, $\boldsymbol{J}$ is the Jacobian matrix with respect to the joint angles $\boldsymbol{q}$, and $\mathbf{K}_q$ has already been defined as a diagonal matrix that aggregates the joint stiffness values in joint space at any given posture.

2.3.3.1.2 Continuous Modelling of Lateral Vibration in Robot Links

A beam experiencing bending can be treated as a *continuous*, or *distributed-parameter system* provided that its mass is not negligible. The application of modal analysis and FEM, which is based on this analytical modelling technique is presented in [21]. In their study, the authors analyzed the vibrations in rectangular plates which were clamped like cantilever beams, however the physical principles, and assumptions that govern this modelling principle were not presented. The mass and stiffness of the continuous system are functions of the spatial variable x and are called distributions. The mass in this distributed case is given as the mass density, ρ or the mass per unit length of the beam. Other systems that can be modelled by this method include strings that are experiencing transverse vibration, rods exposed to axial (longitudinal) vibrations and shafts subjected to torsion.

Since the transverse displacement $y(x,t)$ in these systems depends on two variables, the spatial variable x and time t, which are independent of each other, governing equation of motion for continuous modelling involves partial differential equations which are relatively more difficult to find solutions to, thus requiring some numerical schemes to solve. The governing partial differential equation of motion for strings, rods and shafts are of second-order in a spatial variable x which identifies the nominal position of a point on these elastic members. The motion of a beam, such as the one in figure 2.3 which is experiencing bending in the transverse direction can be described by the partial differential EoM given below, which is based on *Euler-Bernoulli beam theory* [22].

$$-\frac{\partial^2}{\partial x^2}\left[EI(x)\frac{\partial^2 y(x,t)}{\partial x^2}\right] + f(x,t) = m(x)\frac{\partial^2 y(x,t)}{\partial t^2}\ , 0 < x < l \tag{2.23}$$

In the equation above, $y(x,t)$ is the transversal displacement which the beam will experience, $f(x,t)$ is the transversal force which it will experience per unit length, $m(x)$ is the mass of the beam which is distributed per unit of its length, $EI(x)$ is another natural property which represents the beam's flexural rigidity. It can be seen that the motion of the beam is governed by a fourth-order partial deferential equation. In trying to solve this equation, it is necessary to setup a *boundary-value problem* whereby the governing equation must be satisfied over the domain of the system, and the solution $y(x,t)$ of the equation must satisfy four boundary conditions at the end points of the domain - two at each of the beam's left and right boundary.

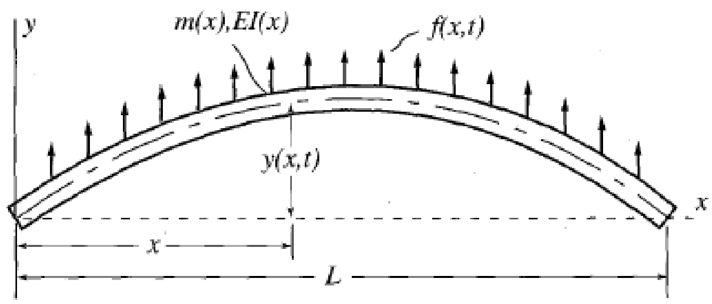

Figure 2. 4: *A beam experiencing bending [22].*

Unlike discrete systems which have a finite number of DoF and modes of vibration, distributed systems possess an infinite number of DoF and infinite number of modes.

2.3.3.1.2.1 Solving the differential Eigenvalue Problem

In order to obtain the natural frequencies and the natural modes of vibration of a free vibrating system which is not experiencing any external forces, the eigenvalue problem for the system must first be solved. For a body that is freely vibrating, a general description of its motion can be given b the equation below.

$$\boldsymbol{M}\ddot{\boldsymbol{q}}(t) + \boldsymbol{K}\boldsymbol{q}(t) = 0 \tag{2.24}$$

Where, M and K are respectively, the system's $n \times n$ mass and stiffness matrices. Also, the general form of eigenvalue problem associated with these mass and stiffness matrices can be expressed as:

$$K\boldsymbol{a} = \omega^2 M\boldsymbol{a} \tag{2.25}$$

Furthermore, for MDoF discrete systems, the algebraic eigenvalue problem can be solved, and a non-trivial solution can be obtained for equation 2.25 if the determinant of the coefficient variables of the eigenvectors, $\boldsymbol{a}$ is equal to zero, which results in a frequency equation.

$$\Delta(\omega^2) = det[K - \omega^2 M] \tag{2.26}$$

Equation 2.26 is known as the frequency equation or characteristic equation of motion of the system and its left-hand side is the characteristic determinant or polynomial of the system. By solving the frequency equation of motion, a set of characteristic values or the roots of the characteristic polynomial which are the approximate eigenvalues, λ_i of the system can be obtained, as well as the eigenvectors, $\boldsymbol{a}_i$ associated with them. The number of eigenvalues that can be obtained from the solution is equal to the number of modes of vibration investigated, or number of DoF of the system. Having obtained the eigenvalues, its square root results in the approximate values for the system's natural frequencies of vibration.

$$\omega_i = \sqrt{\omega_i^2} = \sqrt{\lambda_i} \tag{2.27}$$

Usually in continuous system modelling, directly solving the differential eigenvalue problem to obtain an exact solution comprising an infinite set of eigenvalues is an extremely complex endeavor, hence various approximate methods exist for solving it such as Myklestad's Method and Rayleigh's Energy Method. In this thesis work however, the FEM approach has been adopted which does not require a direct solution to the eigenvalue problem, and is therefore relatively more straightforward and concise. With this analytical procedure, the robotics design engineer can easily obtain the approximate lowest eigenvalue and fundamental natural frequency of vibration of a robot link by approximating it as a beam which is bending due to transverse vibrations. Meirovich presented that this fundamental natural frequency, and the Rayleigh's quotient for a prismatic cantilever beam that is experiencing bending can be expressed in the forms in equation 2.28 and 2.29 respectively, while the stiffness and mass matrices for each finite element of the beam is given in the square matrices in equations 2.30 and 2.31 respectively [22].

$$R(Y_1) = \lambda_1 = \omega_1^2 \tag{2.28}$$

$$R(Y) = \lambda = \omega^2 = \frac{\frac{1}{2}\int_0^L EI(x)\left[\frac{\partial^2 Y(x)}{\partial x^2}\right]^2 dx}{\frac{1}{2}\int_0^L m(x)Y^2(x)dx} \tag{2.29}$$

Cubic interpolation functions were used in the finite element formulation to obtain the elemental stiffness and mass matrices given below. For the matrices, the stiffness and mass distributions of a bending prismatic beam were approximated by assuming that the axial rigidity and mass distributions along the beam are constant in each finite section. The beam's flexural rigidity is given as the product of the its material's modulus of elasticity, E and the moment of inertia of its cross-sectional area, I.

$$K_j = \frac{EI_j n^3}{L^3}\begin{bmatrix} 12 & 6 & -12 & 6 \\ 6 & 4 & -6 & 2 \\ -12 & -6 & 12 & -6 \\ 6 & 2 & -6 & 4 \end{bmatrix} \tag{2.30}$$

$$M_j = \frac{m_j L}{420n}\begin{bmatrix} 156 & 22 & 54 & -13 \\ 22 & 4 & 13 & -3 \\ 54 & 13 & 156 & -22 \\ -13 & -3 & -22 & 4 \end{bmatrix} \tag{2.31}$$

2.4 Integrated Computer Aided Engineering (CAE)

A robot should be designed optimally to obtain a system which all meets all laid out specifications excellently, including high flexural rigidity to help it resist vibrations. However, carrying out this design task is usually a complex endeavor due to the complex nature of its structure and the limitations that arise from the geometries of its links, which are all as a result of the operational expectations of the system. In order to simplify the journey to obtaining an optimal design for their robots, engineers have been adopting the use of CAE techniques. For instance, some best practices for adopting CAE in the design and analysis of several systems including an industrial robot is presented in [11]. However, the theoretical framework which was presented on the robotics system design was limited to basic two-dimensional (2D) kinematics study and structural analysis. Several other literatures exist which have demonstrated the use of this technique in the design lifecycle of robotic systems, for structural modelling and simulations to obtain important information about the systems in order to take vital design decisions which could result in an optimal final design [23],[24].

2.4.1 The Nature of Industrial Robot Design Task

Similar to general engineering design, the robot design process is an iterative and open-ended endeavor [17]. Take for instance, the case of a robotic structure's dynamic behavior which is dependent on its posture, actuator selection is carried out if the structure's frequencies of vibration at a selected set of configurations is acceptable otherwise, a geometrical modification of links and joints is required. For this problem, CAE code such as PTC Creo, Siemens PLM, SOLIDWORKS, CATIA, ANSYS or scientific code such as MATLAB can be used to determine the natural modes of vibration and frequencies of the elastodynamic model at a selected set of robot configurations [17]. The results of the actuator selection can then be incorporated into a final mathematical model which can then be solved by the CAE or scientific code to test the overall performance of the design. By adopting CAE, it is able to better manage this iterative nature of the design tack. The flowchart for an integrated CAE robot design process which can be seen in figure 2.4 was presented in [25],[26]. A modified version of this flowchart, based on the objectives of this study was adapted for this study.

An example of CAE implementation in the design of an industrial robot can be found in [27]. The authors modelled the structure of their robot with SOLIDWORKS, and used ANSYS Workbench for the numerical analysis of their robot structure. However, their work does not include information about the theories that govern the computations that take place within the simulation software or *the blackbox* as it is commonly called, neither did it include methods with which to have an estimate of what the results from the FEM solvers should be or how to verify those results.

By using an integrated CAE approach for robotic design, the design task is made more fluid and flexible, as it becomes possible to more easily manage the iterative nature of the design process since modifications could be easily made to the various part of the robot structure as required after each design stage in the flowchart of figure 24. In order to make use of the technique, it is paramount to have an understanding of the key features of this design technique, which include computer-aided modelling (CAD) and finite element analysis (FEA).

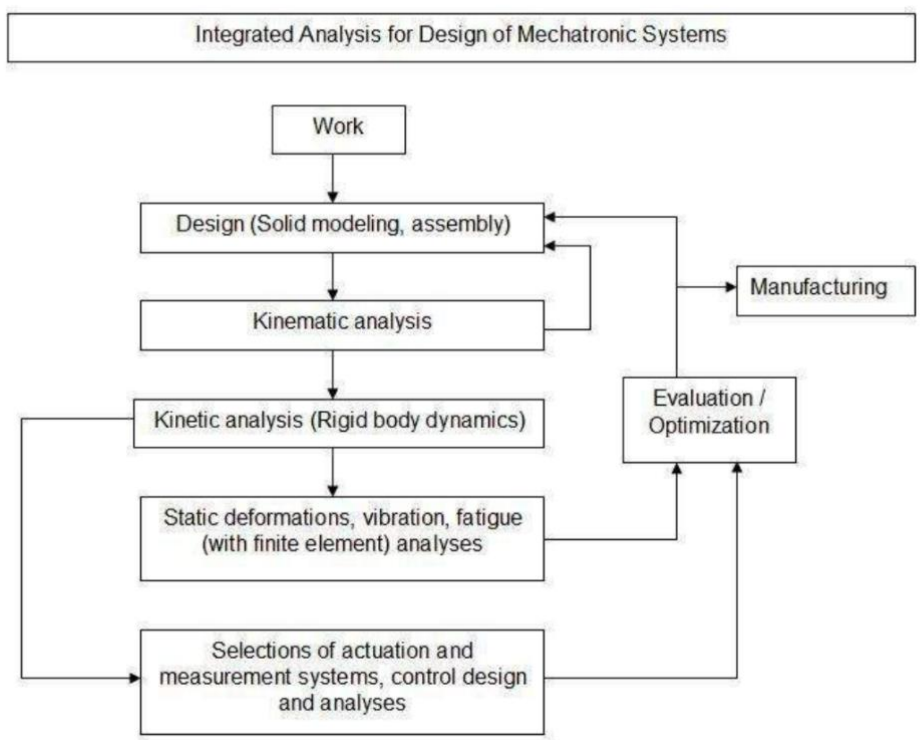

Figure 2. 5: *CAE design flowchart [26].*

2.4.1.1 CAD Modelling

Computer-aided design (CAD) tools have proved to be valuable tools in the field of robotics and will also be employed for this study. Digital data from solid CAD models are used in analysis and simulation of complex robotic structures, as well as for the modelling of its kinetics or rigid body dynamics. With the aid of CAD tools, designers are able to verify designs without having to follow the classical product development process of building physical prototypes during the design phase just for this purpose.

2.4.1.2 Finite Element Analysis (FEA)

To carry out engineering analysis, the physical problem(s) which are to be solved or investigated have to be made into a suitable mathematical model which the simulation software can solve. This mathematical problem, which has assumptions embedded within it, is based on some key physical principles such as equilibrium, conservation, etc. The physical problem(s) determine the user input into the simulation software, such as geometry, mesh, boundary conditions, material properties, etc. These inputs in turn, help the simulation tool to determine the mathematical model that is to be solved. The simulation tool obtains a numerical solution to the mathematical model and obtains selected variables such as displacements, etc. at selected points on the product being simulated. Outside the simulation tool, it is necessary to perform hand calculations based on the physical problem(s). This will give an estimate of what results to expect from the simulation tool. In this study, analytical computations involving frequency equations were carried out during the elastostatical design of the robot to give an estimate of the results to expect from the simulation tool's frequency analysis.

Before concluding the simulation, a systematic process of checking the results through verification and validation has to be carried out. During verification, it is usually checked to see if the numerical results obtained is/are consistent with the mathematical model, if the level of numerical errors is acceptable, and if the results obtained is reasonable in comparison with the results from the hand calculations. Validation on the other hand, involves making sure that the right model was solved, i.e., that the mathematical model is a reasonable representation of the physical problem(s). During the validation stage for this thesis work, it was checked that the mathematical problem was not over simplified, and also that the assumptions embedded in the mathematical model are acceptable, without leaving out important assumptions. Although it is not part of the scope of this work, it is useful to note that apart from comparing the simulation results to the expectations from the hand calculations, the results can also be compared to experimental data during the validation process.

2.5 Summary

It has been presented, that methods such as positional measurement and calibration exist for checking and adjusting the errors in certain parameters that could impact the dynamic characteristics of industrial robots. The most important reasons for such errors have been identified as deflections in the robot's links and joints which mostly arise due to geometric and kinematic design errors. Since a reasonable tread-off has to be made between the weight which the robot can have and the stiffness of its links, it is vital for robotic engineers to be able to take advantage of available opportunities during the robot's geometric and kinematic design, to make important design decisions that will result in optimized robotic systems which will require very minimal or no error investigation or parameter adjustment at all.

The task of designing a robot is known to be mostly tedious, however CAE has been leveraged widely by engineers to make their design task easier. The use of CAE is also advantageous as it blends perfectly with the iterative nature of the design process. However, in most of the literature where the use of this procedures has been presented, the authors fully relied on the numerical results presented by the simulation software to make critical design decisions. This is not very advisable in practice, as it is useful to employ analytical verification techniques for verification of the numerical simulation results. This will also help the robotic design engineer to know important information about the physical principles upon which the numerical simulation results are based, which guide the internal working of their structural system. With this, the engineer can know what kind of results to expect from the simulation ahead of time and what kind of parameters to adjust in the design in order to achieve an optimized structure. A very useful mathematical modelling and approximation technique which can be used for the verification of numerical frequency analysis results is presented in this study.

3 Design Specifications and Process

Most robots used in the industry have six (6) revolute joints with serially-arranged links and the pose of their end-effector is usually varied in 3-dimensional space. For this research work, the robot structure which is designed, analyzed and verified primarily for illustration and proof of concept purposes is designed based on the original design specifications of KUKA KR 15/2 industrial robot, depicted in figure 3.1. This robot was manufactured by German robotics and automation company KUKA AG and is one of such six-axis industrial robots in use which has articulated kinematics capable of all continuous-path controlled tasks. Thus, the main areas of application of the replica robot in this thesis work include machining, product assembly, welding, etc. [5]. The robot is expected to have a relatively low production cost, and be lightweight. However, due to its intended use for CNC machining which requires high precision its structure must be designed such that it will have high resistance to vibrations. Thus, for its structural design, two sets of contrasting conditions must be taken into consideration and trade-offs must be made to obtain an optimized design.

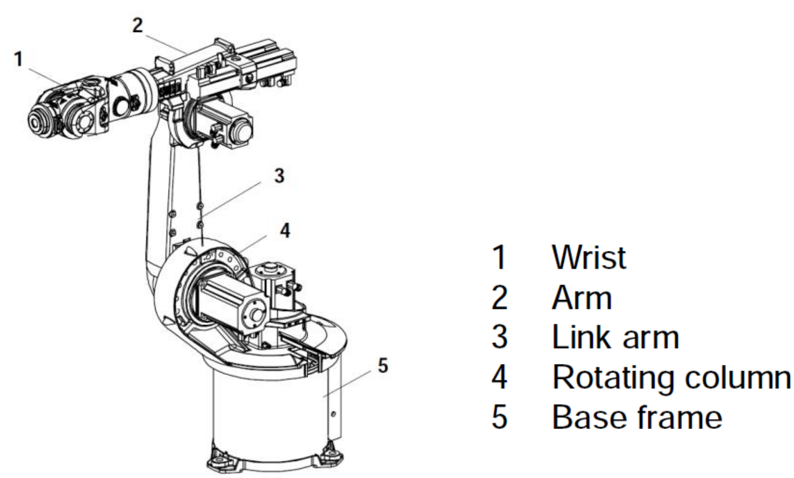

Figure 3. 1: *Main features, based on KUKA KR 15/2 industrial robot [5].*

3.1 Topology of The Industrial Robot

In a typical serial link manipulator such as this one, each joint (or kinematic pair) is attached to the previous joint via a link. The links are rigid bodies, but the robot's sic (6) revolute joints can move. It follows the convention which expects a robot with six (6) joints to have seven (7) links, from its 0^{th} or base link which does not move to the 7^{th} which is the end-effector. As is the case for simple kinematic chains, apart from the base and link seven (7) every other link is connected to the previous and next link by the robot's joints, while each of those five (5) links connects two joints, thus making up six (6) two-pair axes with possible movements depicted in figure 3.2 [5]. The first mobile part of the robot is the rotating column which is mounted on top of the fixed base frame. This link rotates about the vertical (z) axis of the robot and when it does, it turns other links along with it. The end-effector which could be a machining tool for example, will be attached to a mounting flange at the wrist.

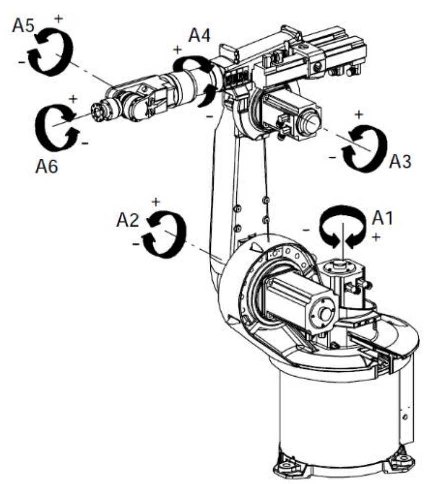

Figure 3. 2: *Rotational axes and directions of rotation, based on KUKA KR 15/2 robot [5].*

3.2 Operating Capacity of The Industrial Robot

Some important parameters to decide on from the onset of an industrial robot design endeavor include the volume of the robot's workspace, its rated payload and the desired velocities for its axes. An industrial robot's workspace is the set of all possible positions that its end-effector can reach, and factors that influence this include the dimensions of the robot arm and the mechanical limits on the range of motion of particular joints. The robot control software also prevents parts of the robot arm from colliding or intersecting with other parts of the robot's arm or its base, hence the presence of volume around the robot body where it cannot reach. The shape and dimensions of the robot's working envelope is presented in figure 3.3, which is adapted from the data sheet of the KUKA KR 15/2 [3]. The image has a plan view and side elevation view of the robot, with information of the it's reachable and unreachable volumes. The maximum reach for the robot is $1570mm$, and the volume of its working envelope is approximately $13.1 \times 10^9 mm^3$. With its construction, the robot is expected to accommodate a $15kg$ rated payload on its wrist and a maximum of 10kg supplementary load on its arm [3]. The working envelope shows the dimensions of the robot's principal axis, as well as the conditions for loading the robot.

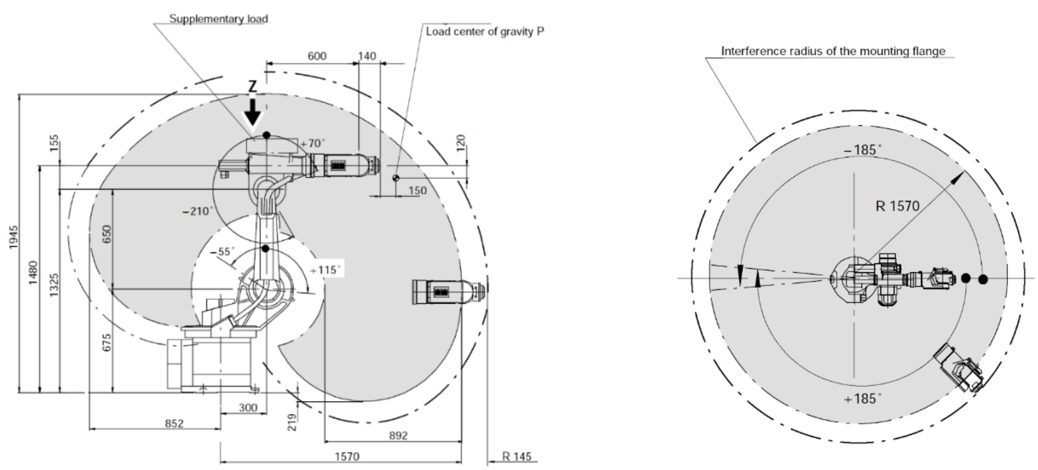

Figure 3. 3: *Workspace and work envelope, based on KUKA KR 15/2 industrial robot [5].*

3.3 Manufacture of The Industrial Robot

In designing the robot, important factors such as its expected operating environment and required structural strength are dully considered, as well of constraints such as cost effectiveness, lightweight and high rigidity which influenced the material selection for its manufacture. Due to its precision with positioning control, a low-inertia AC servomotor which is transistor-controlled will be used for the actuation of each axis of the robot developed in this study. The cost of these motors increase proportionally as their torque rating increases, thus if extremely rigid and heavy links are used which will require more power due to high torque motors, requirements for lightweight construction and low-cost construction will not be met. Therefore, a balance has to be struck between the structure's rigidity and the allowable weight for the links.

Table 3. 1: Properties of Aluminium 6061 Alloy.

Property	**Value**
Elastic Modulus (E)	$69000\ N/mm^2$
Mass Density (ρ)	$2.7 \times 10^{-6}\ Kg/mm^3$
Tensile Strength (F_{tu})	$124.084\ N/mm^2$
Yield Strength (σ_y)	$55.1485\ N/mm^2$
Poisson's Ratio (ν)	0.33

For this industrial robot design study, Aluminum 6061 which is a light cast alloy material has been selected. This is a similar material to that which was used in the manufacture of the KUKA KR15/2 robot, and some its important properties are presented in table 3.1. The base and links, which make up the robot's moving principal assemblies will be made of this material. They will be manufactured individually by casting and machining to their desired shape, after which they will all be assembled together into a single mechanical system, followed by the attachment of components such as the actuators and electronic peripherals to give the robot an approximate total weight of $237Kg$. This material is obviously not as rigid as steel since it is an alloy of Aluminum, hence before proceeding to its manufacture, it is vital to carry out vibrational analysis in order to ensure that the material of the robot, as well as the geometry of the inks will be capable of resisting as much as possible, the detrimental vibrations that could occur in the robot's links due to rapid movements to and from its destination positions while in operation.

3.4 Integrated Computer-Aided Design

The CAE approach to designing a complete robotic system was presented as a flowchart in figure 2.4, however since for this study the focus is on the design of the robot's mechanical structure, a modified flowchart of the CAE-guided activities contained in the design task of this study can be found below.

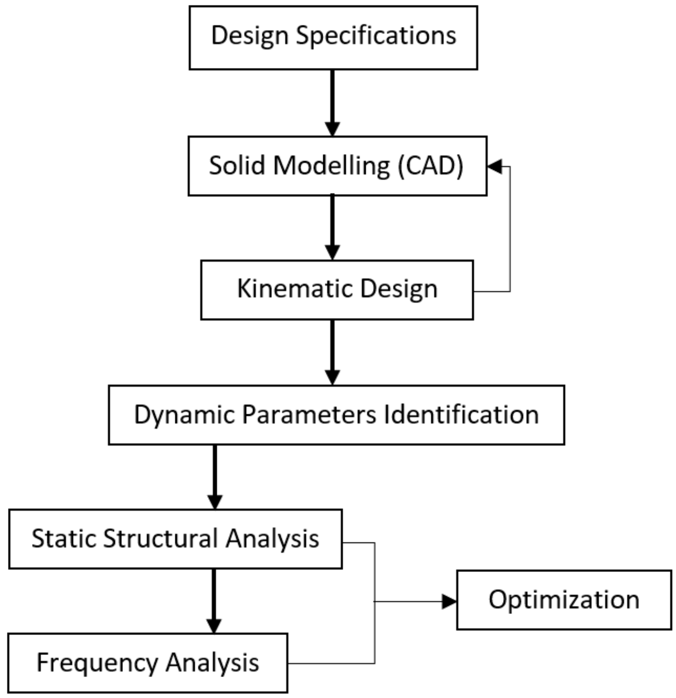

Figure 3. 4: *Modified design flowchart.*

From the flowchart, the iterative nature of the design process can be seen which is a common characteristic of any engineering design task. For instance, it will be seen that a geometrical modification of the initial links and joints design was required after the kinematic and rigid body dynamics design of the robot. For this report however, all the design stages mentioned in the flowchart have be outlined sequentially starting with the design specifications and CAD modelling. For this thesis work, the engineering modelling environment of PTC Creo and SOLIDWORKS integrated FEA software tools were employed for CAD modelling and numerical static structural and vibrational analyses, while MATLAB was used during elastostatic modelling to aid with complex analytic mathematical computations involving frequency equations, of which the results were used to verify some numerical results obtained from the simulation tool's FEM code.

4 Structural Design Process

This chapter contains information regarding the mechanical design process which was embarked upon to create the main structure of the robot. All the steps taken at different stages are laid out in details, including the kinematic design and verification, dynamical design, and vibrational characteristics modelling.

4.1 Geometrical Characteristics and Forward Kinematics (FK)

To describe a robotic end-effector's position and orientation (or the robot's pose), a coordinate frame has to be attached to it. The position of the robot can then be described by the position of that coordinate frame's origin, while the angles between the pose's coordinate frame and the reference coordinate frame describes its orientation. In solving the FK problem, the pose of a robot's EE can be described as a chain or sequence of elementary homogeneous transformation matrices (containing translations and rotations for 3D-space). However, for this to be obtained, geometric dimensioning of the robot has to be carried out, from which the architecture of the robot can be determined which will further help in determining its configuration or posture. In carrying out geometric modeling of this type of a robotic manipulator, using the kinematic chains is the simplest approach; and for this kinematic chain to be conveniently described, the D–H notation which was introduced in Chapter 2 has been used here.

In the D-H notation, the link transform is represented by a homogeneous transformation matrix, A. The matrix is made up of some elementary transformations: a rotation about the z-axis, a translation along the z-axis, a translation along the x-axis and finally, a rotation about the x-axis. This is a key aspect of the notation; the relationship between two link coordinate frames can be described by four (4) parameters: θ, d, a and α (2 rotations and two translations) rather than six (6) which a pose of a robot link is made of.

$$^{j-1}\xi_j \sim A = R_z(\theta_j)T_z(d_j)T_X(a_j)R_x(\alpha_J) \tag{4.1}$$

where:

$\xi \subset SE(3)$

$i = 1, \dots, 6$

$T \subset SE(3)$: in 3D space, T is a subset of all the EE's possible positions and orientations,

$\xi_E \in T$: the EE pose belongs to a set of T (a set or space of all possible EE poses), and

$\xi_E \sim \left(x, y, z, \theta_r, \theta_p, \theta_y\right)$: position and orientation

The elementary matrices in the homogeneous transformation matrix of 4.1, when expanded out with all transformations multiplied together results in a single 4x4 homogeneous transformation matrix which represents the relative pose between consecutive link reference frames with respect to the link coordinate frame of the joint. The 4x4 homogeneous transformation matrix will comprise of a translational part, which represents the position of the EE (its x, y, z coordinates) of the robot and a rotational part which indicates the orientation of the of the EE and is a function of the sum of all the robot's joint angles ($\sum_{i=1}^{n} q_i$). Generally, for manipulators in 3-Dimensional Space a symbolic expression for their homogeneous transformation matrix has a 3x3 rotational component and a 3x1 translational component. All the matrices belong the set of all rotations and translations in 3-dimensional space.

$$T = \begin{bmatrix} R & t \\ 0,0,0 & 1 \end{bmatrix} \tag{4.2}$$

4.1.1 Populating the D-H Parameters Table

The principal dimensions and working envelope of the 6-axis robot can be seen in figure 3.3, from which a desirable configuration of the robot is shown. In accordance with the D–H notation, seven coordinate frames have been defined on the robot in figure 4.1 with F_1 fixed to the base and F_7 to the far end of the EE. The corresponding link parameters (D-H parameters) for the coordinate systems established in the figure can be found in table 4.1.

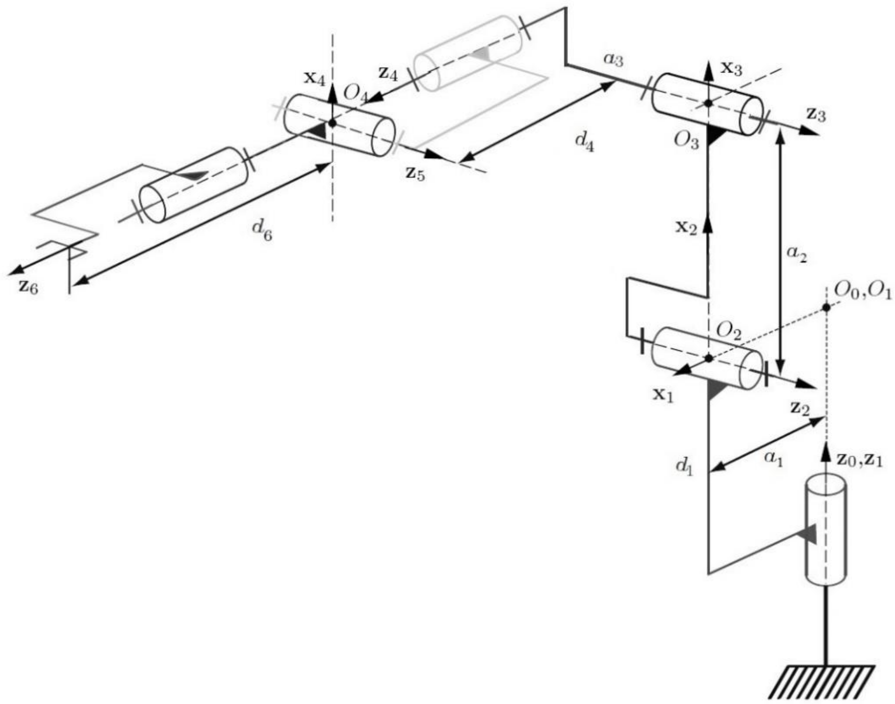

Figure 4. 1: *Geometrical reference frames of the robot.*

The following rules have been followed in order to arrive at the D-H parameters:

a. Joint angle (θ_r) is the angle from x_{i-1} to x_i measured about z_{i-1},
b. Joint offset (d_j) is the distance from the origin of $i-1$ coordinate frame to the intersection of z_{i-1} and x_i axes, measured along z_i axis,
c. Link length (a_j) is the distance between z_{i-1} and z_i axes, measured along x_i axis i.e., distance from the intersection of z_{i-1} and x_i axes to the origin of the i^{th} coordinate frame, measured along x_i axis,
d. Link twist angle (α_j) is the angle from z_{i-1} to z_i measured about x_i.

Table 4.1 contains the 18 constant D-H parameters, which fully define the architecture of the manipulator. These D-H parameters have been used in this study, alongside the 6 joint variables (*joint coordinates)*, which are grouped in the 6-dimensional vector $\boldsymbol{q}$, to fully define the robot's configuration, or posture. Thus, the D-H parameters, when combined with the joint coordinates will uniquely define the industrial robotic manipulator’s pose.

Table 4. 1: Geometric Dimensions of the Robot (D-H Parameters Table).

Joint axis (i)	Joint angle $\boldsymbol{\theta_r}$ [°]	Joint offset $\boldsymbol{d_j}$ [m]	Link length $\boldsymbol{a_j}$ [m]	Link twist angle $\boldsymbol{\alpha_j}$ [°]
1	q_1	0.6750	0.3000	$+90$
2	q_2	0.0000	0.6500	0
3	q_3	0.0000	0.1550	$+90$
4	q_4	0.6000	0.0000	-90
5	q_5	0.0000	0.0000	$+90$
6	q_6	0.1400	0.0000	0

The joint angles q_1 to q_6 are variables and are taken as the generalized coordinates of the system, while a_j, d_j and α_J are constant parameters which are functions of the mechanical design of the robot. The robot only has revolute joints; hence its joint angles make up the $\boldsymbol{\theta}$ values in equation 4.3. As the robot is made to move, only the joint angles or θ values change, while all the other D-H parameters remain constant.

General mathematical notation:

$$\xi_N = \mathcal{K}(\boldsymbol{q}; \boldsymbol{\theta}, d, a, \alpha, \sigma) \tag{4.3}$$

$$\text{If } \sigma_j = \begin{cases} R \longrightarrow \theta_j = q_J \\ P \longrightarrow d_j = q_j \end{cases}$$

Where, ξ is the pose of the end-effector and the subscript N represents the number of joints of the robot, $\mathcal{K}$is a function which stands for FK (it operates on the robot joint angles and returns the robot pose), $\boldsymbol{q}$ is the joint configuration (vector of N-joint variables), $\boldsymbol{\theta}$ represents joint angles, d represents link offsets, a represents link lengths, α represents link twists, σ represents joint types, R represents revolute joint, and P represents prismatic joint. Thus, the FK equation which describes the pose of a serial-link manipulator can be written succinctly as shown below.

$$\xi = \mathcal{K}(q) \tag{4.4}$$

4.1.2 Homogeneous Transformation Matrix for the Robot

A 6-link manipulator can reach any particular position in its workspace, and there are several joint angle configurations that will result in different EE orientations but the same EE position. The principal goal of forward kinematics is to obtain a single matrix which describes the relationship between the base frame of the robot and its EE. To accomplish this for a 6-dof robot, six (6) groups of the four (4) 4x4 elementary transformation matrices in equation 4.1 can be stacked (multiplied by each other), each group containing four (4) parameters which describe the relationship between one link frame of the robot and the next. Each elementary transformation matrix represents the relative pose from one link frame of the robot to the next. Considering that the robot has six (6) joints and seven (7) coordinate frames attached to it, a combination of all the homogeneous transformation matrices will yield an expression which will fully define the pose of the robot's end-effector, which will be a large 4x4 homogeneous transformation matrix. This matrix will represent the forward kinematics transformation matrix for the robotic manipulator from its end-effector to its base frame. Finally, from this matrix, the robot end-effector's pose can be extracted. The general form of translational and rotational matrices below has been used alongside the parameters in the D-H table given above to expand the homogeneous transformation matrix in equation 4.1.

General form of the homogeneous translation transform operator:

$$\boldsymbol{T}(t) = \begin{bmatrix} 1 & 0 & 0 & t_x \\ 0 & 1 & 0 & t_y \\ 0 & 0 & 1 & t_z \\ 0 & 0 & 0 & 1 \end{bmatrix} \tag{4.5}$$

Where, $t = \sqrt{t_x^2 + t_y^2 + t_z^2}$, and t_x, t_y, t_z are components of the translation vector.

General form of the homogeneous rotation transforms operators about the z and x axes:

$$R_z(q_i) = \begin{bmatrix} cosq_i & -sinq_i & 0 \\ sinq_i & cosq_i & 0 \\ 0 & 0 & 1 \end{bmatrix} \tag{4.6}$$

$$R_x(\alpha_i) = \begin{bmatrix} 1 & 0 & 0 \\ 0 & cos\alpha_i & -sin\alpha_i \\ 0 & sin\alpha_i & cos\alpha_i \end{bmatrix} \tag{4.7}$$

Upon expansion, the general form of each of the six (6) homogeneous transformation matrices will be of the form below:

$$^{i-1}T_i = \begin{bmatrix} cosq_i & -sinq_i.cos\alpha_i & sinq_i.sin\alpha_i & a_i.cosq_i \\ sinq_i & cosq_i.cos\alpha_i & -cosq_i.sin\alpha_i & a_i.sinq_i \\ 0 & sin\alpha_i & cos\alpha_i & d_i \\ 0 & 0 & 0 & 1 \end{bmatrix} \tag{4.8}$$

The expression above represents the general form of the homogeneous transformation matrix from one link frame of the robot to the next. When compared with the general symbolic expression in equation 4.2 for manipulators in 3-dimensional space, it can be identified that the elements of the top left 3×3 matrix is the 3×3 rotational component of the robot's pose which describes its orientation, while the elements of the 3×1 matrix on the right is the translational component of the robot's pose which describes its position.

4.1.3 The Forward Kinematics Implementation

The use of the expression in equation 4.8 to compute the pose of the robot's end-effector is presented in this sub-section. As seen in equation 4.9, the equation for the robot's kinematics design requires stacking up six such homogeneous transformations. The elements of each of the six matrices are parameters which are obtained from the D-H table (table 4.1).

$$^{0}T_{6} = \prod_{i=1}^{6} {}^{i-1}T_{i} \tag{4.9}$$

Where, the trailing subscript i and the leading superscript $i-1$ denotes that the transformation takes place from the i^{th} coordinate system to the robot's $(i-1)^{th}$ coordinate system. By adapting equation 4.8 and substituting the link parameters listed in the D-H table, the six (6) homogeneous transformation matrices from each link transformation to the next are presented below:

$$^{0}T_{1} = \begin{bmatrix} cosq_1 & 0 & sinq_1 & 0.3.cosq_1 \\ sinq_1 & 0 & -cosq_1 & 0.3.sinq_1 \\ 0 & 1 & 0 & 0.675 \\ 0 & 0 & 0 & 1 \end{bmatrix} \tag{4.10}$$

$$^{1}T_{2} = \begin{bmatrix} cosq_2 & -sinq_2 & 0 & 0.650.cosq_2 \\ sinq_2 & cosq_2 & 0 & 0.650.sinq_2 \\ 0 & 0 & 1 & 0 \\ 0 & 0 & 0 & 1 \end{bmatrix} \tag{4.11}$$

$$^{2}T_{3} = \begin{bmatrix} cosq_3 & 0 & sinq_3 & 0.155.cosq_3 \\ sinq_3 & 0 & -cosq_3 & 0.155.sinq_3 \\ 0 & 1 & 0 & 0 \\ 0 & 0 & 0 & 1 \end{bmatrix} \tag{4.12}$$

$$^{3}T_{4} = \begin{bmatrix} cosq_4 & 0 & -sinq_4 & 0 \\ sinq_4 & 0 & cosq_4 & 0 \\ 0 & -1 & 0 & 0.600 \\ 0 & 0 & 0 & 1 \end{bmatrix} \tag{4.13}$$

$$
{}^{4}T_{5} = \begin{bmatrix} cosq_5 & 0 & sinq_5 & 0 \\ sinq_5 & 0 & -cosq_5 & 0 \\ 0 & 1 & 0 & 0 \\ 0 & 0 & 0 & 1 \end{bmatrix} \tag{4.14}
$$

$$
{}^{5}T_{6} = \begin{bmatrix} cosq_6 & -sinq_6 & 0 & 0 \\ sinq_6 & cosq_6 & 0 & 0 \\ 0 & 0 & 1 & 0.140 \\ 0 & 0 & 0 & 1 \end{bmatrix} \tag{4.15}
$$

By carrying out the computation in 4.9, the large 4x4 matrix ${}^{0}T_{6}$ which describes the pose of the robot's end-effector was obtained. Upon comparing 4.8 with 4.2, the homogeneous transformation matrix with 3×3 rotational component and a 3×1 translational component, which fully describes the orientation and position of the robot's end-effector relative to its base frame can be written in the form of 4.16. For the industrial robot designed in this study, complete expressions for the elements of the matrix presented below can be found in Appendix A1.

$$
{}^{0}T_{6} = \begin{bmatrix} r_{x1} & r_{x2} & r_{x3} & t_x \\ r_{y1} & r_{y2} & r_{y3} & t_y \\ r_{z1} & r_{z2} & r_{z3} & t_z \\ 0 & 0 & 0 & 1 \end{bmatrix} \tag{4.16}
$$

4.1.3.1 Verification of the Forward Kinematics

In order to verify the result of the analytical computation above, open-source MATLAB Robotics Toolbox was used here to carry out numerical forward kinematics computations for the robot in order to compare the results with those obtained from analytical computations [20]. With the software tool, the D-H parameters were defined, which are displayed in table form as shown in figure 4.2, after which a *'SerialLink'* robot object was created which represents the robotic manipulator in the workspace of the toolbox. With this robot object setup, several functions could be performed on it in order to interact with the robot and study its behavior. To carry out the verification, both numerical and analytical evaluations had to be carried out for different configurations of the robot and compared against each other.

Research Robot:: 6 axis, RRRRRR, stdDH, slowRNE

j	theta	d	a	alpha	offset
1	q1	0.675	0.3	1.5708	0
2	q2	0	0.65	0	0
3	q3	0	0.155	1.5708	0
4	q4	0.6	0	-1.5708	0
5	q5	0	0	1.5708	0
6	q6	0.14	0	0	0

Figure 4. 2: *D-H parameters table obtained from MATLAB Robotics Toolbox.*

In Chapter 3 the working envelope of the robot was presented, showing the dimensions of its principal axis and the conditions for loading the robot, which can be seen in below in figure 4.3. During numerical structural analysis, it is important to take these loading conditions into consideration. In order to properly setup a virtual representation of the load in the simulation tool at the specified location, the pose of the robot's end effector must be known for each of the configurations that the robot will be simulated. Hence, to carry out the verification it was reasonable to compute the forward kinematics for the two configurations of the robot which will be structurally simulated in Chapter 4.

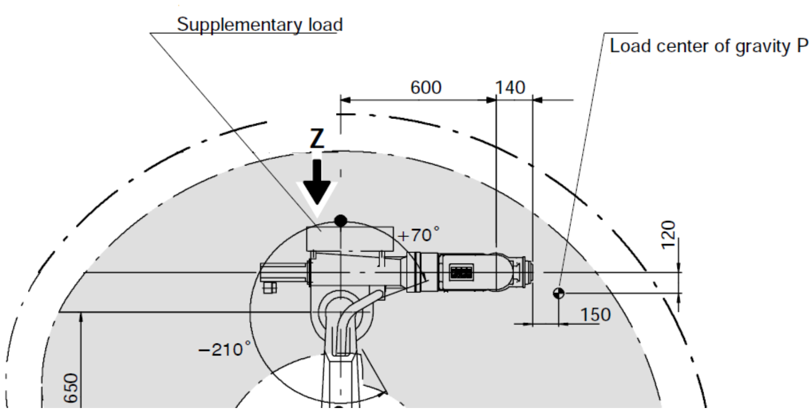

Figure 4. 3: *Specifications for loading the Robot [3].*

For the first configuration, the pose of the robot's end-effector is such that all the robot's joint angles are at 0^0 except for joint angle q_2 which is at 90^0 (1.5708 radians). In this pose, the robot is expected to be able to move fluidly in different directions hence why it was chosen for this comparison. For the second configuration, all the angles of the robot are locked at 0^0 except for joint angle q_3 which is at 90^0 (1.5708 radians). This configuration is important since it enables the robot to achieve its maximum reach. More importantly, it is essential to carry out structural simulations in this second configuration of the robot since it represents a critical loading condition for parts of the robotic structure, especially the link arm and the rotating column.

4.1.3.1.1 Numerical Implementation

By using the MATLAB robotics toolbox function *'teach'*, the line of code below was implemented to graphically display these desired configurations of the robot and it can be seen in figure 4.4.

$$Research\_Robot.teach([0\ 1.5708\ 0\ 0\ 0\ 0]); \tag{4.17}$$

$$Research\_Robot.teach([0\ 0\ 1.5708\ 0\ 0\ 0]); \tag{4.18}$$

From the result, the pose of the robot's end-effector at both configurations were obtained as seen below. Next in the verification procedure was to compare these results against the analytical computation results which can be found in the next sub-section.

$$Research\_Robot\_Conf1 = \begin{bmatrix} 1.0400 \\ -0.0000 \\ 1.4800 \end{bmatrix} \tag{4.19}$$

$$Research\_Robot\_Conf2 = \begin{bmatrix} 1.6900 \\ 0.0000 \\ 0.8300 \end{bmatrix} \tag{4.20}$$

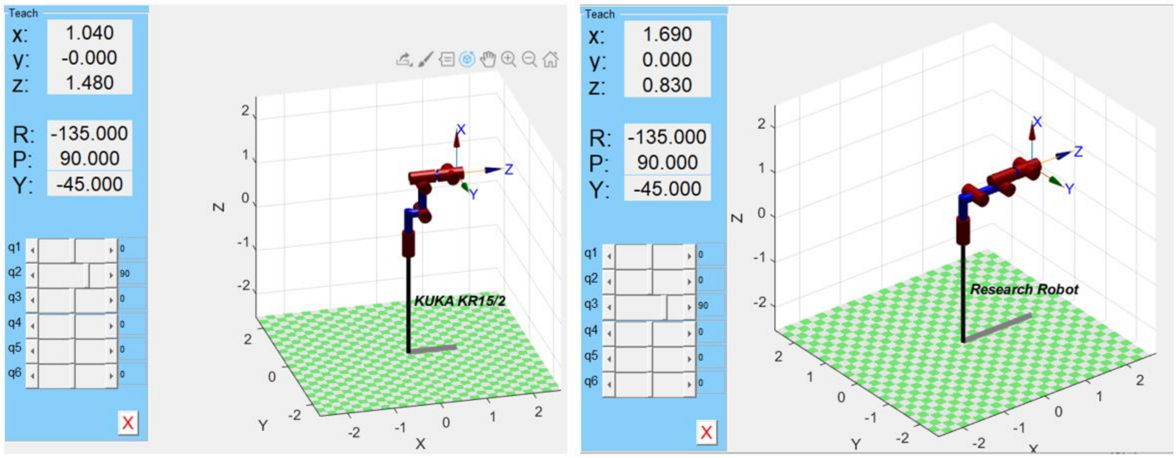

Figure 4. 4: *Graphical models of robot configurations from MATLAB Robotics Toolbox.*

4.1.3.1.2 Analytical Implementation

The mathematical expressions which are the elements of the FK matrix in equation 4.8, can be found in Appendix A). In order to verify their accuracy, the equation was implemented in a MATLAB function to compute the FK of the robot at the two configurations by varying the angular terms in the expressions. To execute the FK, the formulated functions were executed with the MATLAB method *'fkine'*. The lines of code can be seen below, as well as the result of the Robotic Toolbox's computation which is the homogeneous transformation matrix that describes the EE pose or the robot's forward kinematics at each of the configurations.

$$Research\_Robot\_Ver1 = Research\_Robot.fkine([0\ 1.5708\ 0\ 0\ 0\ 0]); \tag{4.21}$$

$$Research\_Robot\_Ver1 = \begin{bmatrix} -0.0000 & 0.0000 & 1.0000 & 1.040 \\ -0.0000 & -1.0000 & 0.0000 & -0 \\ 1.0000 & -0.0000 & 0.0000 & 1.480 \\ 0 & 0 & 0 & 1 \end{bmatrix} \tag{4.22}$$

$$Research\_Robot\_Ver2 = Research\_Robot.fkine([0\ 0\ 1.5708\ 0\ 0\ 0]); \tag{4.23}$$

$$Research\_Robot\_Ver2 = \begin{bmatrix} -0.0000 & 0.0000 & 1.0000 & 1.6900 \\ -0.0000 & -1.0000 & 0.0000 & 0.0000 \\ 1.0000 & -0.0000 & 0.0000 & 0.8300 \\ 0 & 0 & 0 & 1 \end{bmatrix} \quad (4.24)$$

From the expressions above, it is obvious that result obtained by using the derived forward kinematics equation to compute the end-effector poses agreed with the result provided by the Robotics Toolbox computation. The first 3×3 elements represent the orientation of the robot's end-effector, while the last 3×1 are the x, y and z coordinates of the robot's end-effector position. With this, the accuracy forward kinematics which was derived in as equation 4.16 has been verified, and important information about the pose of the robot's end-effector which will be required for structural simulations has also been obtained. The detailed MATLAB code which was written for this verification procedure can be found in Appendix A2.

4.2 Dynamics

Although it will be more useful for the control system design which is outside the scope of this study, it is however important to lay out as many of the dynamic characteristics (kinetics) of the industrial robot system as possible. This information will be useful for planned future work to achieve a complete design of the robot, which will involve control systems design and topology optimization. For the actuation selection, which will require designing a feedback control system for the robot, the equations of motion for the system must be formulated. These are second-order linear differential equations which will serve as the system's transfer function to be solved during the modelling in order to obtain important information that will aid the controller design. To obtain these equations of motion however, the system's kinetic and potential energies must be computed. Computing the kinetic energy as it was presented in Chapter 2 requires knowledge of the velocities of the centers of masses of the robotic structure's six (6) links, which is part of what is being presented in this section.

4.2.1 Dynamical Parameters

Generally, the dynamic properties of a rigid body can be fully determined by three (3) quantities:

a. The body mass m which is a scalar quantity,
b. The position vector $\boldsymbol{r}_c$ of the rigid body's center of mass, and
c. The inertia tensor $\boldsymbol{I}$ with respect to the rigid body's center of mass.

However, specifically for a serial-link industrial robotic manipulator, each of its links will have 10 parameters which include:

a. The mass, m_i of the i^{th} link which is a scalar quantity,
b. The x_{c_i}, y_{c_i} and z_{c_i} coordinates of the position vector, ${}^0\boldsymbol{r}_{c_i}$ of the i^{th} link's center of mass with respect to the base coordinate frame, and
c. The six (6) independent entries in the inertia tensor $\boldsymbol{I}_i$ with respect to the i^{th} link's center of mass, expressed in terms of the inertia coordinate frame.

Hence, sixty (60) dynamic parameters must be identified in order to completely describe a 6-link industrial robot, all of which can be obtained or computed with the aid of information from the CAD model of the robot.

4.2.1.1 Robot Material and Total Mass

The robot in this study has similar geometric properties as the KUKA KR15/2 robot which was manufactured of cast light alloy and has an approximate mass of $235Kg$. In order to ensure that the robot in this study has similar mass, then it has to be manufactured of a similar material. To this end, Aluminium 6061 alloy was selected, and its properties can be found in section 3.3. In order to determine the mass of the virtual robot model which can be found in Chapter 5, the selected material was assigned to it in the CAD software, which gave the robot model an approximate mass of $237Kg$. The mass, m_i of each of the robot's links can be obtained from the CAD model.

4.2.1.2 Robot's Links CoM Position Vector

The position vector of a rigid body's CoM is usually defined in the body-fixed frame and its origin is regarded as the body's geometrical reference point, as a consequence the components of the vector are constant for rigid bodies. The point ${}^{i}r_{c_i}$ located in link i, which describes the position of the center of mass of the i^{th} link with respect to the link's fixed frame (i^{th} frame) can be described by the position vector expression below, where the number 1 in the 4^{th} row is included so as to aid the homogeneous transformation computation when computing for the position vector, ${}^{0}r_{c_i}$ of the i^{th} link's center of mass with respect to the base coordinate frame.

$$ {}^{i}r_{c_i} = \begin{bmatrix} {}^{i}x_{c_i} \\ {}^{i}y_{c_i} \\ {}^{i}z_{c_i} \\ 1 \end{bmatrix} = \begin{bmatrix} {}^{i}x_{c_i} & {}^{i}y_{c_i} & {}^{i}z_{c_i} & 1 \end{bmatrix}^T \tag{4.25} $$

From the CAD model, the position vector ${}^{i}r_{c_i}$ was obtained for each of the robot's links and is presented in table 4.2.

Table 4. 2: Centers of Mass of The Robot's Links.

Link (i)	**Center of Mass, ${}^{i}r_{c_i}$ (m)**
0 (Base frame)	$(-0.0261, -0.0001, 0.1649)$
A1 (Rotating Column)	$(0.1662, 0.0023, 0.1460)$
A2 (Link Arm)	$(0.0000, 0.3067, 0.0479)$
A3 (Arm)	$(-0.1259, 0.0002, -0.0245)$
A4 (Lower Wrist)	$(0.7743, 0.0307, 1.4502)$
A5 + A6 (Wrist)	$(0.0288, 0.0000, 0.0691)$
A7 (Gripper)	$(0.0680, 0.0000, 0.0000)$

4.2.1.3 Inertia Tensor

The inertia tensor was mentioned in Chapter 2 of this report. These parameters for each link will have six (6) independent entries in the matrix, and are expressed in the robot's body-fixed frame, centered at the center of mass of the links. However, in computing the dynamics of the robot with the Lagrangian approach, all the parameters of the robot have to be expressed in terms of generalized coordinates. Hence, as with the velocities, $\vec{v}_{C_i}$ of the links' centers of mass, the moment of inertia will be expressed with respect to the base coordinate frame (inertial frame). This can be accomplished by multiplying each of the links' inertia matrix by the rotation matrix, R which denotes the rotation between the link's body fixed frame to the inertial frame, and its transpose, R^T as expressed below.

$$\mathbf{I}_i = R_i(\boldsymbol{q}) I_i R_i(\boldsymbol{q})^T \tag{4.26}$$

From the CAD model of the robot, the inertia tensor of each of the robot's links (expressed in equation 2.15) can be obtained.

4.2.1.4 Velocities of Robot Links' Centers of Masses

The center of mass of a robot link which is described with respect to the world coordinate frame with its origin at point O can be considered as a point fixed on the robot link which can be represented by the position vector, $\vec{r}_{C_i}$. The velocity of this point, $\vec{v}_{C_i}$ expressed with respect to the base coordinate frame is used for the computation of the robot's kinetic energy during its dynamical modelling. As seen in 4.27, it will be obtained by taking the first derivatives of the position vectors, ${}^0r_{c_i}$.

$${}^0v_{c_i} = v_{c_i} = \frac{\partial}{\partial t}\left({}^0r_{c_i}\right) = \frac{\partial}{\partial t}\left({}^0T_i \cdot {}^ir_{c_i}\right) \tag{4.27}$$

Where ${}^0r_{c_i}$ is the position vector describing the center of mass of the i^{th} link with respect to the base coordinate frame, and ${}^ir_{c_i}$ which has been obtained already from the robot's CAD model and is presented in table 4.2 is the position vector describing the center of mass of the i^{th} link with respect to the link's fixed frame (i^{th} frame). ${}^{0}v_{c_i}$ is the velocity of the i^{th} link with respect to the base coordinate frame, and ${}^{0}T_i$ is a matrix of homogeneous transformation from the base of the robot to the link in consideration, a general form of this matrix for a single transformation can be seen in equation 4.8. For a six-link robot, six (6) of the expressions in equation 4.8 are required to describe ${}^{0}T_i$ which will be expressed in the following form:

$$ {}^{0}T_i = {}^{0}T_6 = {}^{0}T_1 {}^{1}T_2 {}^{2}T_3 {}^{3}T_4 {}^{4}T_5 {}^{5}T_6 \tag{4.28} $$

It can be observed that the expression in 2.19 above will evaluate to the expression below for each link of a 6-link robot:

$$ v_{c_i} = \left(\sum_{j=1}^{i} \frac{\partial {}^{0}T_i}{\partial q_j} \dot{q}_j \right) {}^{i}r_{c_i} \tag{4.29} $$

where: $i = j = 1, 2, 3, 4, 5, 6$ is the link and joint number respectively.

The partial derivative of the general form of the homogeneous transformation matrix in 2.9 can be descried by the expression below:

$$ \frac{\partial {}^{i-1}T_i}{\partial q_j} = Q_i {}^{i-1}T_i \tag{4.30} $$

Where the matrix Q_i for rotary joints is:

$$ Q_i = \begin{bmatrix} 0 & -1 & 0 & 0 \\ 1 & 0 & 0 & 0 \\ 0 & 0 & 0 & 0 \\ 0 & 0 & 0 & 0 \end{bmatrix} \tag{4.31} $$

Hence, as a general form:

$$ \frac{\partial {}^{i-1}T_i}{\partial q_j} = \begin{bmatrix} 0 & -1 & 0 & 0 \\ 1 & 0 & 0 & 0 \\ 0 & 0 & 0 & 0 \\ 0 & 0 & 0 & 0 \end{bmatrix} \begin{bmatrix} cosq_i & -sinq_i.cos\alpha_i & sinq_i.sin\alpha_i & a_i.cosq_i \\ sinq_i & cosq_i.cos\alpha_i & -cosq_i.sin\alpha_i & a_i.sinq_i \\ 0 & sin\alpha_i & cos\alpha_i & d_i \\ 0 & 0 & 0 & 1 \end{bmatrix} \tag{4.32} $$

The partial derivatives of the homogeneous transformation matrix of link i with respect to the joint angles j which can be seen in 2.21 above can be expanded thus:

$$U_{ij} = \frac{\partial\, {}^0T_i}{\partial q_j} = \ {}^0T_1 \ldots\ {}^{j-2}T_{j-1}\, Q_j\, {}^{j-1}T_j \ldots {}^{i-1}T_i \tag{4.33}$$

The above expression comprises of three (3) parts which can be seen below:

$$U_{ij} = \left({}^0T_{j-1}\right) Q_j \left({}^{j-1}T_i\right) \tag{4.34}$$

Thus, equation of the velocity for the center of mass of the i^{th} link with respect to the base coordinate frame is:

$$v_{c_i} = \left(\sum_{j=1}^{i} U_{ij}\, \dot{q}_j\right) {}^i r_{c_i} \tag{4.35}$$

For a 6-link robot, the following expressions can be used for the computation of each link's center of mass velocities.

For link 1, where $i = 1, j = 1$:

$$\sum_{j=1}^{i} U_{ij} = \ U_{11} = \frac{\partial\, {}^0T_1}{\partial q_1} = \ Q_1\, {}^0T_1 \tag{4.36a}$$

For link 2, where $i = 2, j = 1, 2$:

$$\sum_{j=1}^{i} U_{ij} = \ U_{21} + U_{22} \tag{4.36b}$$

For link 3, where $i = 3, j = 1, 2, 3$:

$$\sum_{j=1}^{i} U_{ij} = \ U_{31} + U_{32} + U_{33} \tag{4.36c}$$

For link 4, where $i = 4, j = 1, 2, 3, 4$:

$$\sum_{j=1}^{i} U_{ij} = \ U_{41} + U_{42} + U_{43} + U_{44} \tag{4.36d}$$

For link 5, where $i = 5$, $j = 1, 2, 3, 4, 5$:

$$\sum_{j=1}^{i} U_{ij} = U_{51} + U_{52} + U_{53} + U_{54} + U_{55} \tag{4.36e}$$

For link 6, where $i = 6$, $j = 1, 2, 3, 4, 5, 6$:

$$\sum_{j=1}^{i} U_{ij} = U_{61} + U_{62} + U_{63} + U_{64} + U_{65} + U_{66} \tag{4.36f}$$

By following the expressions summarized above in 4.36a to 4.36f, the centers of mass of each of the robot's links were obtained. The resulting matrices are functions of the robot's joint angles. The complete set of expressions for the computation are quite complex and long and the MATLAB code which was used for the computations is available in Appendix A2.

4.3 Elastostatic Modelling

In this sub-section, attention is drawn to the elastostatic modelling of the vibrations which could occur on the robot's links. The design objective here was to achieve a maximum permissible value for the possible minimum lateral natural frequency of vibration that could be experienced in the robot's link arm. In the configuration where the robot has its maximum reach, the link arm is kept in a horizontal position and it is locked at joint q_3, therefore it can be treated as a beam member. Thus, a proposed approximate solution to the eigenvalue problem of a cantilever beam experiencing transversal bending is presented in this section.

The transversal mode of vibration occurs in the direction perpendicular to the length of the beam, causing the beam to bend and its centerline to shift away from its ideal position. Therefore, for a robotic arm which experiences such vibrations, it will be difficult to achieve accuracy of operation, and even more detrimental is the case whereby the robot is exposed to very low resonant frequencies which could eventually lead to structural failure of the system. Care should be taken by the robot designer that the natural frequency of transversal mode of vibrations in the robot's links do not coincide with its frequency of vibration when it is subjected to external forces. A preliminary study is presented below for a transversely bending beam model, which will serve as a basis for the analytical hand calculations in Chapter 5 for the vibrations in the industrial robot's link arm.

4.3.1 The Boundary Value Problem

In order to obtain the eigenvalue problem, first a boundary value problem has to be setup by assuming that the beam is a continuous system with distributed mass and stiffness along its length. It is also assumed that it is vibrating freely without any external excitations. Thus, to setup the boundary-value problem, $f(x,t)$ which represents the distributed force in the general PDE of motion is eliminated from equation 2.24 to obtain the new equation 4.37 for transverse displacement $y(x,t)$ of a freely bending beam.

$$-\frac{\partial^2}{\partial x^2}\left[EI(x)\frac{\partial^2 y(x,t)}{\partial x^2}\right] = m(x)\frac{\partial^2 y(x,t)}{\partial t^2}\ ,0 < x < l \tag{4.37}$$

For the preliminary study, a relatively simpler model was considered which involves the cantilever beam in figure 4.5. The beam is fixed at $x = 0$ and free at $x = L$ and is assumed to be experiencing bending due to transverse vibrations. Of course, this system has slightly different boundary conditions from one having a lumped mass at its free end which would provide a better representation for the link arm vibration computation presented in Chapter 5. Since two boundary conditions (BCs) must be satisfied at each of the two ends of the beam by the solution of the partial differential equation $y(x,t)$, the boundary conditions presented below in equations 4.38a to 4.38d were considered for this preliminary study.

Two geometric BCs at the left boundary:

i. No bending displacement (deflection):

$$y(x,t) = 0 \tag{4.38a}$$

ii. Slope of deflection is equal to zero:

$$\frac{\partial y(x,t)}{\partial x} = 0 \tag{4.38b}$$

Two natural BCs at right boundary:

iii. No bending moment:

$$M(x,t) = EI(x)\frac{\partial^2 y(x,t)}{\partial x^2} = 0 \tag{4.38c}$$

iv. Shearing force:

$$Q(x,t) = -\frac{\partial}{\partial x}\left[EI(x)\frac{\partial^2 y(x,t)}{\partial x^2}\right] = 0 \tag{4.38d}$$

The solution to equation 4.37 is the body's axial displacement, which is harmonic in nature and has the form shown below in equation 4.39.

$$y(x,t) = CY(x)\cos(\omega t - \phi) \tag{4.39}$$

Where, C is a constant term which represents the beams amplitude, $Y(x)$ is the displacement profile of the beam in y direction occurring at distances x from its clamped end. For the other terms, ω is the natural frequency of vibration of the system, and ϕ represents phase angle. Equation 4.39 which describes a conservative system's free vibration serves as a trial function with which the system at hand could be solved.

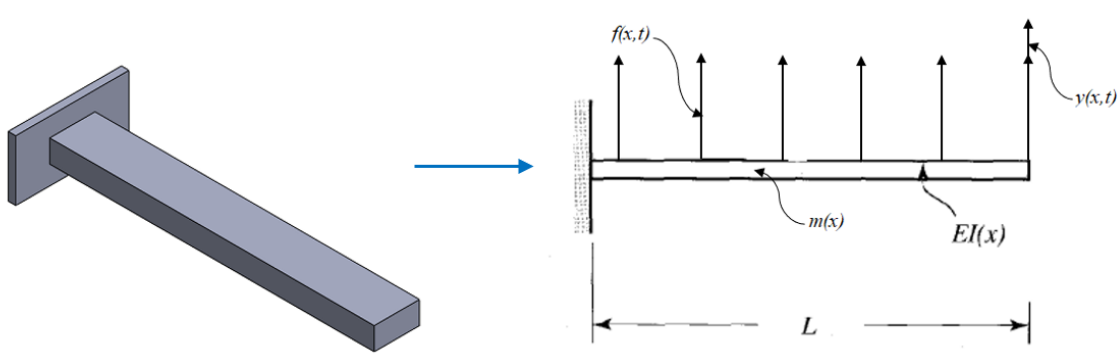

Figure 4. 5: *A freely vibrating cantilever beam.*

4.3.2 The Eigenvalue Problem

The differential eigenvalue problem for a modelling a beam's vibrations comprises of one differential equation and four boundary conditions. The partial differential equation was obtained by inserting the trial function in equation 4.39 into equation 4.37 and dividing through both sides of the equation by $C\cos(\omega t - \phi)$.

$$\frac{d^2}{dx^2}\left[EI(x)\frac{d^2Y(x)}{dx^2}\right] = \omega^2 m(x)Y(x)\,, 0 < x < l \tag{4.40}$$

The BCs:

Two geometric BCs at the left boundary, $x = 0$:

i. No bending displacement (deflection):

$$Y(x) = 0 \tag{4.41a}$$

ii. Slope of deflection is equal to zero:

$$\frac{dY(x)}{dx} = 0 \tag{4.41b}$$

Two natural BCs at right boundary, $x = l$:

iii. No bending moment:

$$M(x) = EI(x)\frac{d^2Y(x)}{dx^2} = 0 \tag{4.41c}$$

iv. Shearing force:

$$Q(x) = -\frac{d}{dx}\left[EI(x)\frac{d^2Y(x)}{dx^2}\right] = 0 \tag{4.41d}$$

4.3.2.1 Solution to the Eigenvalue Problem

An approximate solution to the eigenvalue problem is presented here which involves an FEM approach, based on Rayleigh's quotient. By using Rayleigh's principle, it would not be necessary for the design engineer to directly compute the solution to the differential eigenvalue problem. For practical purposes such as the one in this design study, the most vital information required is the fundamental natural frequency of the vibrating system, which is its lowest natural frequency obtained from the lowest eigenvalue. Therefore, the analytical FEM procedure which is presented here has been used to obtain an excellent approximation of this important information for the beam in question, considering the boundary conditions that have been laid out already. The fundamental natural frequency and the Rayleigh's quotient for this system were given in equations 2.28 and 2.29 respectively.

The objective is to solve the eigenvalue problem by first evaluating the mass and stiffness matrices, which in turn can be substituted into the equation 2.25. This will then be evaluated numerically to obtain the eigenvalues of the vibrating body. With the eigenvalues obtained, the body's natural frequencies of vibration and the modes can be easily computed. The FEM approach to solving the eigenvalue problem requires discretization of the beam into finite elements and numerically deriving the *elemental* stiffness and mass matrices, after which the *global* stiffness and mass matrices can be constructed for the whole system by implementing what is known as an *assembly procedure*. For this work, all these have been carried out by using the MATLAB computer program and the scripts have been made available in Appendix B1 which can be found at the end of this report.

4.3.2.1.1 Evaluating the Stiffness and Mass Matrices

From the Rayleigh's quotient expression in equation 2.29, the numerator is maximum potential energy, P_{max} of the system. This integral is evaluated to obtain the 4×4 stiffness matrix in equation 2.30 for each finite element by introducing third-order interpolation. Also, the 4×4 mass matrix for each finite element given in equation 2.31 was obtained from the denominator integral, which is the reference kinetic energy of the system, E_{ref}. To solve the eigenvalue problem, a MATLAB program was written which can be found in Appendix B1, for the construction of the global stiffness and mass matrices.

In MATLAB FEM code implementation, the beam was discretized into ten (10) elements. Within the code, the assembly procedure was carried out to obtain the global matrices, and with the rows and columns of the matrices struck out as required by the laid down boundary conditions the result was two 20×20 square global stiffness and mass matrices. With the appropriate matrices obtained, the MATLAB function, '*eig()*' was invoked to carry out the numerical evaluation of equation 2.25. The approximate lowest eigenvalue, λ_1 was obtained from the MATLAB code to be 3.5160 while the approximate natural frequencies for the second and third modes of vibration, λ_2 and λ_3 were 22.0352 and 61.7129 respectively. The plotted mode shapes can be found in figure 4.6.

In general, the closed form of the natural radial frequency of a beam in transverse vibration can be expressed as:

$$\omega_n = \lambda_i \sqrt{\frac{EI}{mL^4}} \tag{4.42}$$

The natural linear frequency of a beam in transverse vibration is related to its natural radial frequency in the form given below:

$$f_n = \frac{\omega_n}{2\pi} \tag{4.43}$$

When the natural frequencies that were evaluated with the MATLAB code were inputted into equation 4.44, it was obtained that the fundamental natural radial frequency and the first two overtones for any arbitrary prismatic beam which is experiencing transversal bending can be evaluated as shown below in equations 4.44b and 4.44c. Larger overtones can be evaluated by using the natural frequency values from the MATLAB code as required. By assigning some values for the geometric and natural parameters, the fundamental linear natural frequency as well as higher linear natural frequencies (overtones) for a vibrating prismatic beam experiencing transverse bending can be obtained.

$$f_1 = \frac{3.5160}{2\pi}\sqrt{\frac{EI}{mL^4}} \tag{4.44a}$$

$$f_2 = \frac{22.0340}{2\pi}\sqrt{\frac{EI}{mL^4}} \tag{4.44b}$$

$$f_3 = \frac{61.7000}{2\pi}\sqrt{\frac{EI}{mL^4}} \tag{4.44c}$$

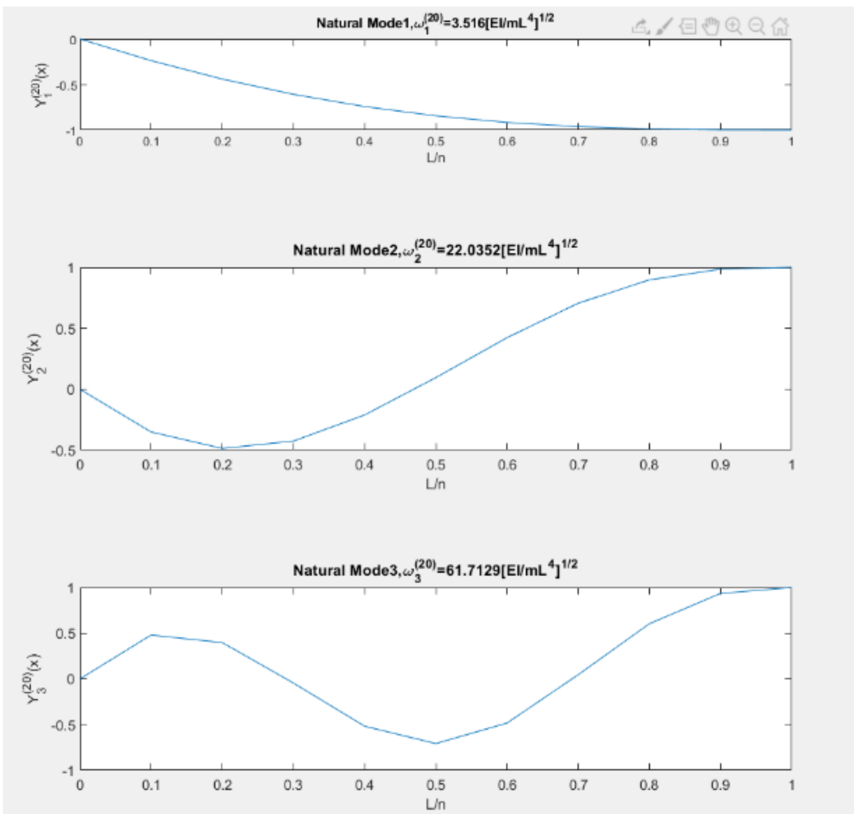

Figure 4. 6: *The first three (3) mode shapes.*

5 CAE Design and Verification

A critical task embedded into the scope of this study was to carry out numerical analyses of the robot design, which included static structural and modal analysis. From these analyses, several important data can be obtained from the model such as regions of high stresses and displacements, as well as its structural rigidity under various load cases. In order to effectively tackle this problem, FEM code of SOLIDWORKS was used. The analyses carried out include a static structural analysis on the CAD model of the robot. before a frequency analysis was also carried out. The steps which were followed for the setup and evaluation of these numerical studies, as well as verification techniques are outlined in the sections that ensue.

5.1 3D CAD Modelling

In order to obtain data for design tasks such as kinematics and kinetic modelling, as well as to enable the proposed numerical simulations for this work to be carried out, a virtual version (or digital twin) of the robot had to be built. Within the scope of this thesis work, building this virtual version of the robot involved producing a three-dimensional (3D) CAD model of the robot. To accomplish this, the rigid base and links of the robot arm were modelled and assembled using the solid modelling tool in SOLIDWORKS integrated CAE software. The tools embedded within this software can be used for three-dimensional (3D) mechanical design, product simulation, analysis and testing, of discrete manufactured products etc.

5.1.1 Robot Links Identification and CAD Modelling

As a general rule, if a motion takes place between two components, both components will be considered in the multibody model as two separate bodies, connected by a joint. The first step when modelling a Multi-Body System (MBS) is the identification of the bodies. The bodies that make up the robot are assumed to be rigid, hence it was modelled as a rigid assembly of multiple bodies. The bodies or links include the base frame, rotating column, link arm, arm and the lower and upper wrists. In order to obtain more realistic simulation results, a sufficiently detailed model is advisable. The models of the robot's base and links which can be found on table 5.1 were made to look as closely as the real robot's links would appear, and they will play important roles during the course of this study. Closely accurate dynamical information about the robot can extracted from the software, such as the centers of mass for each of its links, the moments of inertia, etc. which will be used in computations for the robot's dynamical design. Furthermore, this model will serve as the virtual version of the robot on which finite element analysis will be carried out in order to simulate the structural and to predict the dynamical behaviors of the actual robot, etc.

Table 5. 1: 3D Models of Robot's Base, Links and Actuators.

Identifier	**Name**	**3D model**
A0	*Base frame*	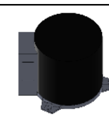
A1	*Rotating column*	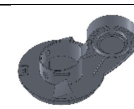
A2	*Link arm*	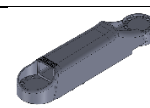
A3	*Arm*	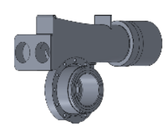
A4	*Lower wrist*	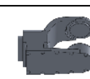
A5 + A6	*Wrist*	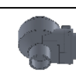
M1	*Motor 1*	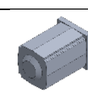
M2	*Motor 2*	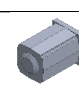
M3	*Motor 3*	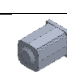

It was necessary to select electric motors which can bear the weights of the robot's links to serve as actuators which will drive the robot's axes. Since this work is primarily focused on the structural design, motor selection has not been explicitly carried out. In the structural analysis however, it is vital to take the influence of the motors' weights on the robot's joints and overall structure into account. For a good estimate of the masses of these motors, the robot structure in this design was set to have an approximate maximum mass of $237Kg$, which is within the range of the approximate total mass of the KUKA KR15/2 robot. Thus, it was assumed that the motor torques required to drive both robots' axes will be approximately similar. This assumption provides an upper limit for the motor torques required for the robot's actuation.

Provided that the robot's structural design is sufficient, which will be decided from the static structural simulation, the torque requirement can only be made lower in the case that topology optimization is carried out to reduce the mass of the robot's links. Topology optimization is not in the scope of this present study; however, it is proposed as part of a future study in order to achieve a more complete and optimized design which will more sufficiently satisfy the design specifications for the industrial robotic manipulator. With these conditions set and assumptions made, motors with similar weight used by the KUKA KR15/2, due to the similarities in their size and in the Aluminium alloy material of their shells or housing were modelled, which have been included in table 5.1 and can also be observed in the assembled robot below.

Figure 5. 1: *3D model of the assembled industrial robot.*

5.2 Finite Element Analysis (FEA) and Verification

Analysis that will be carried out will include static structural analysis to help in studying and making important decisions about the system's capability to withstand loads, modal analysis to aid in numerically investigating the robot's rigidity which will be compared with analytical hand calculations for verification purposes. Both analyses were carried out in order to investigate the mechanical behavior of the real system when it is being loaded to its maximum capacity at two different configurations. Information on each of these simulation studies are discussed in this section of this report.

5.2.1 Static Structural Analysis of the Robot

In order to investigate the capacity of the robot structure to withstand automated and high-speed and precision manufacturing tasks, its virtual model has been subjected to computer-aided static structural analysis. The analysis was carried out for two possible working configurations of the robot for which its kinematics was computed in Chapter 4. The configuration where the robot's axes were locked in a fixed position and its pose was confined such that joint angle q_2 was kept at 90^0, and others were kept at 0^0 was simulated as configuration one, since in this configuration the robot should expect less stress than in the second configuration where it has the maximum reach. The study setup and results of the analyses which were carried out, such as the stresses and displacements experienced by the structure, as well as the design decision that was taken as a result of the insights obtained from the simulation tools will be discussed in this sub-section.

5.2.1.1 Simulation Study Setup

The main steps for setting up the numerical simulation task include importing the CAD model that is to be simulated, simplifying its topology, applying the right material to it, assigning constraints and external loading to the body, performing meshing, and finally getting the tool to carry out the analysis. These steps which followed in order to accomplish the task have been outlined below.

5.2.1.1.1 Model Preparation and Material Assignment

To carry out the static structural analysis, the CAD model of the robot at the desired configuration was imported into SOLIDWORKS simulation environment. Some minor features which would have had little or no effect on the result were taken off the original model in order to obtain a neater and simpler model which the FEM solver could evaluate without running into errors. After correctly setting up the desired configuration, Aluminium 6061 alloy material, which was already presented in Chapter 3 was identified in the CAD tool and assigned to all the parts of the robot structure. The motors were assigned with Aluminium 6063-T5 alloy material.

5.2.1.1.2 Constraint and Loading

It had to be ensured that the physical situation of the system was represented as closely as possible in the simulation. A fixture constraint was attached to the base of the robot to simulate the real-life mounting position of the robot in the manufacturing floor. Furthermore, the effect of gravity on the structure was taken into account as an external load, while the maximum allowable supplementary load of $10Kg$, and maximum allowable payload of $15Kg$ were respectively assigned in a vertical downward direction to the robot’s arm and the location of its end-effector as shown in figure 4.3. For the allowable $15Kg$ payload, the conditions laid out in the specifications had to be taken into consideration. With the use of the results of the kinematics computation where the pose of the robot was obtained for two configurations, the mounting condition for the mass at both configurations were obtained as follows.

$$\text{EE } load\ position\ 1 = \begin{bmatrix} 1.040 \\ 0 \\ 1.480 \end{bmatrix} + \begin{bmatrix} 0.150 \\ 0 \\ -0.120 \end{bmatrix} = \begin{bmatrix} 1.190 \\ 0 \\ 1.360 \end{bmatrix} \tag{5.1}$$

$$\text{EE } Load\ position\ 2 = \begin{bmatrix} 1.6900 \\ 0 \\ 0.8300 \end{bmatrix} + \begin{bmatrix} 0.150 \\ 0 \\ -0.120 \end{bmatrix} = \begin{bmatrix} 1.8400 \\ 0 \\ 0.7100 \end{bmatrix} \tag{5.2}$$

5.2.1.1.3 Meshing

For this analysis, different sizes of a 4-node-element tetrahedral mesh was employed by the software to mesh the different parts of the model. A representation of this mesh element type can be seen below.

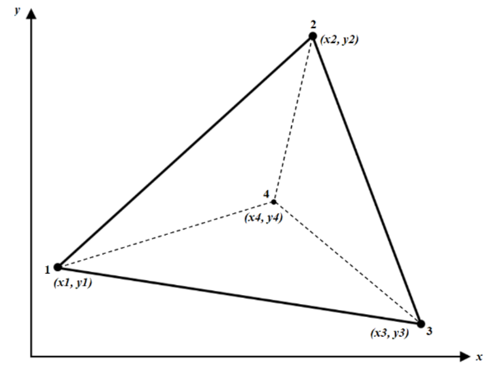

Figure 5. 2: *A 4-node tetrahedral mesh element.*

The robot model configuration one (1), its meshing outcome, the constraint as well as the loading conditions as it appeared in the simulation environment can be seen below in figure 5.3.

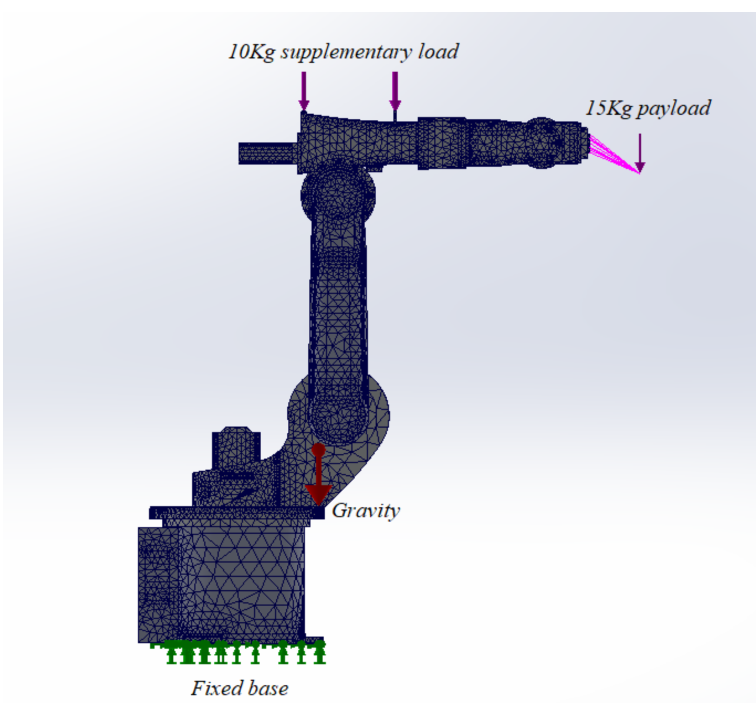

Figure 5. 3: *Meshed model of the robot in configuration one (1).*

5.2.1.2 Computation and Results

After setting-up the study, the simulation tool was made to generate and solve the mathematical model for this problem and present the results which enabled post-processing to be carried out. Important simulation results of the static structural analysis for stresses and displacements experienced by the robot model under the prescribed configuration and load case were plotted graphically by the software.

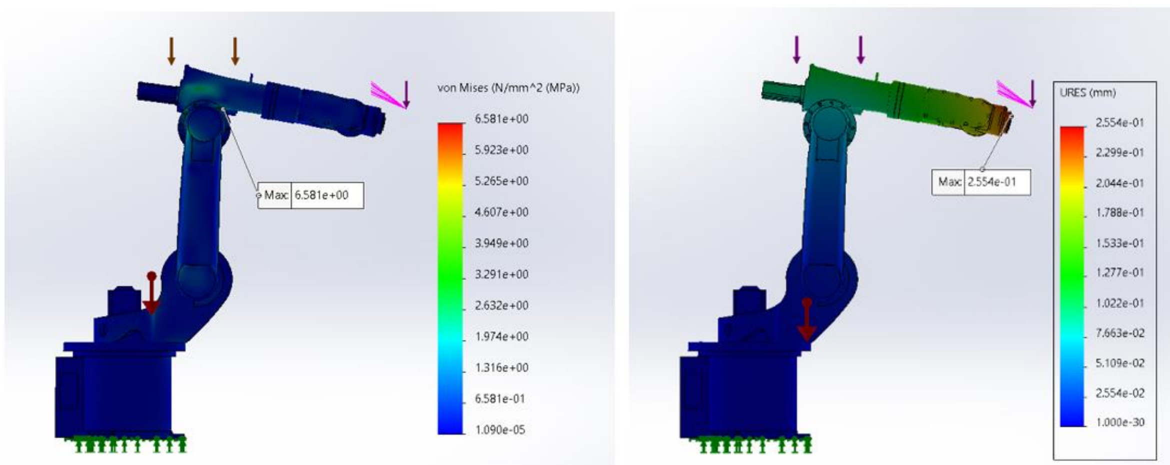

Figure 5. 4: *Graphical plot of the stresses and displacements in robot configuration one (1).*

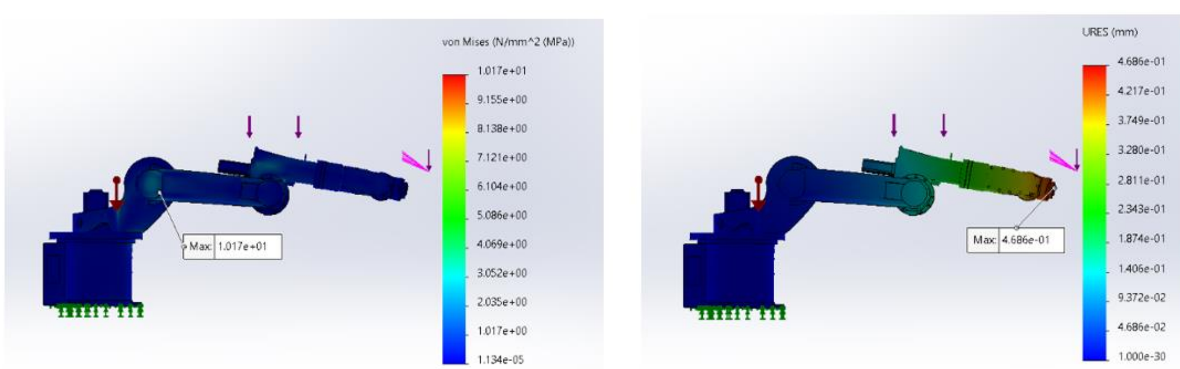

Figure 5. 5: *Graphical plot of the stresses and displacements in robot configuration two (2).*

The scaled-up graphical representations of the simulation results can be seen in figures 5.4 and 5.5, where according to the results it can be seen that for configuration one (1) and two (2), the maximum von Mises stress that is experienced on the overall arm, which is being considered as a failure criterion for the model is approximately $6.58MPa$ and $10.17MPa$ respectively, which are both considerably lower than Aluminium 6061 Alloy's approximate yield strength of $55.15MPa$. This suggests that the structure of the robot is very capable of handling the recommended maximum loading of $25Kg$ at both configurations. Furthermore, the maximum resultant displacement of $0.26mm$ and $0.47mm$ respectively for both configurations which is experienced at the mounting flange of the robot as expected, are both within the allowable displacement limit for the robotic structure.

Having obtained excellent static structural characteristics from the simulation results, the next step was to carry out investigations which could reveal the dynamical behavior of the structure. This was carried out with the aid of frequency analysis, which is the content of the next sub-section.

5.2.2 Frequency Analysis of the Robot

Frequency analysis gives results such as the natural frequencies and mode shapes of a vibrating body, which provide information about dynamical loading characteristics of that body. With it, important conclusion can be drawn regarding the stiffness of the structure that makes up the body. At its natural frequency of vibration, the system tends to vibrate even without experiencing any driving or damping force. The devastating consequence of vibrations in structures is the state of resonance which leads to total failure of a system. However, for a robotic system which is highly sensitive and requires excellent levels of accuracy, even vibrations above resonant frequencies of vibration can impact the system negatively. Therefore, it is essential to ensure that the first mode of vibration of a robotic system has a natural frequency of vibration which is acceptably high.

In this sub-section, the numerical results of the frequency analysis as well as a graphical representation of some of the lowest modes of vibration of the complete robot structure is presented. Design decisions which were taken based on the information gotten from these results has also been pointed out.

5.2.2.1 Simulation Study Setup

Since the simulation required a similar setup to that of static structural analysis presented above, the old setup and mesh was copied to the new one. This is one of the advantages of using an integrated CAE tool for engineering design. However, since the frequency of vibration depends on a system's mass and stiffness, no loading was applied to the system for this analysis setup.

5.2.2.2 Computation and Results

After the setup, the software was made to carry out the computations and present the simulation results. Natural frequency results of the robot model for the first four (4) modes of vibration can be found in table 5.2 for both simulated configurations.

Table 5. 2: Results of Frequency Analysis.

	Natural Frequencies (Hz)	
Modes	**Configuration 1**	**Configuration 2**
1	28.9630	26.6600
2	44.9910	42.6060
3	65.4280	88.4080
4	100.5500	132.8200

In the case of vibrations, the failure criterion is the state of resonance whereby the system is found to be vibrating at extremely low natural frequencies. If the system vibrates at a frequency that is close to or matches its lowest natural frequency when forced, this could lead to resonance. Thus, it is important for the system's lowest natural frequency to be as high as possible such that a forcing element which would be vibrating at a much lower frequency would have no adverse effect on the dynamics and the structure of the system.

From the graphical plots of the robot's mode shapes which can be found in figures 5.6 and 5.7, it can be observed that in modes one (1) and two (2), the vibrations at the wrist of the robot causes the link arm, arm and wrist sub-assembly to bend in the horizontal and vertical plane respectively. In modes three (3) and four (4), the arm experiences vibrations which cause the link arm, arm and wrist sub-assembly to experience torsion. The natural frequency results presented in table 5.2 are high, hence the robot is sufficiently rigid and its accuracy will not be impacted much by the structure's vibrations.

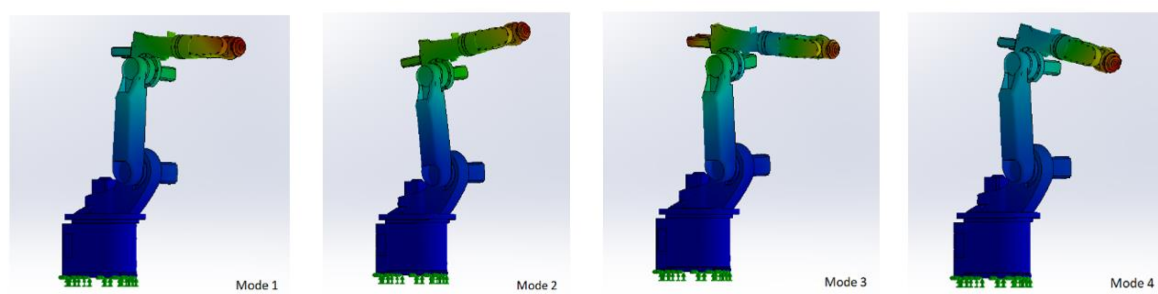

Figure 5. 6: *Graphical plots for the first four (4) mode shapes of robot configuration one (1).*

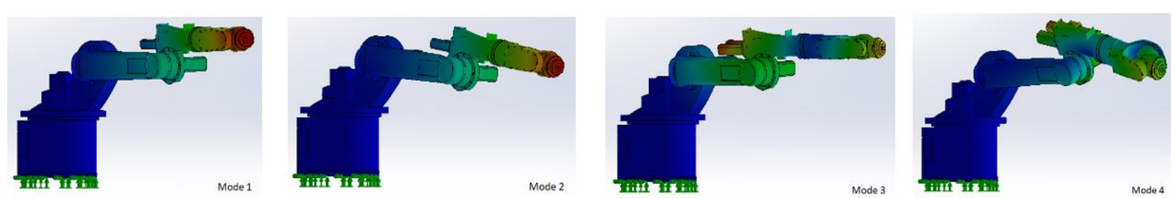

Figure 5. 7: *Graphical plots for the first four (4) mode shapes of robot configuration two (2).*

5.2.3 Mathematical Modelling and Analysis of Vibrations in Link Arm

In this section a mathematical model is presented which provides an estimate of the dynamic behavior of the robot's link arm. A task like this helps the robot designer to have an idea about what to expect from the numerical analysis without fully depending on whatever the simulation tool or *Blackbox* gives as a result. The link arm is the most susceptible to resonant frequencies since it is located right at the center of the robotic structure and it bears the weight of the links and motors that come after it, as well as the external loading that will be applied to the robot while it is in operation.

By following systems modelling approach, the link arm shown in figure 5.8, when it is locked at joint q_2 can be approximated to be a uniformly distributed cantilever beam which is experiencing lateral vibration. Furthermore, the complicated solid models which represent the rest of the robot's links can be replaced with an equivalent model by applying a concentrated mass at the right end of the link arm (joint q_3) which will represent the totality of the masses of the arm, lower wrist, wrist, gripper, and motors. The objective here was to obtain the eigenvalues of this representative system by solving its eigenvalue problem analytically, from which the system's natural frequencies of vibration could be obtained by evaluating equation 4.48. The computation presented here involves elements of the preliminary computation which was carried out in section Chapter 4 for a fixed-free cantilever beam of uniform cross-section. However, to correctly represent the physical condition of the link arm, a more closely approximate model is proposed and evaluated.

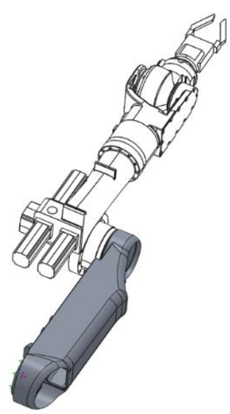

Figure 5. 8: *The arm, lower wrist, wrist and motors attached to link arm at joint* q_3.

5.2.3.1 Link Arm Eigenvalue Problem

The fourth-order partial differential equation for the differential eigenvalue problem of a vibrating beam was presented in Chapter 2. For the link arm approximation, the four boundary conditions given in Chapter 3 will have a minor modification to include a lumped mass at the free right boundary of the beam. Thus, the representative beam in figure 5.9 has been assumed to be fixed at $x = 0$ and free but with a lumped mass, m at $x = L$. The lateral displacement, which is given by the solution $y(x,t)$ of the partial differential equation is expected to satisfy the boundary conditions laid out below:

Two geometric BCs at the left boundary, $x = 0$:

i. No bending displacement (deflection):

$$Y(x) = 0 \tag{5.3a}$$

ii. Slope of deflection is equal to zero:

$$\frac{dY(x)}{dx} = 0 \tag{5.3b}$$

Two natural BCs at right boundary, $x = l$:

iii. No bending moment:

$$M(x) = EI(x)\frac{d^2Y(x)}{dx^2} = 0 \tag{5.3c}$$

iv. Shearing force:

$$Q(x) = \omega^2 MY(x) + \frac{d}{dx}\left[EI(x)\frac{d^2Y(x)}{dx^2}\right] = 0 \tag{5.3d}$$

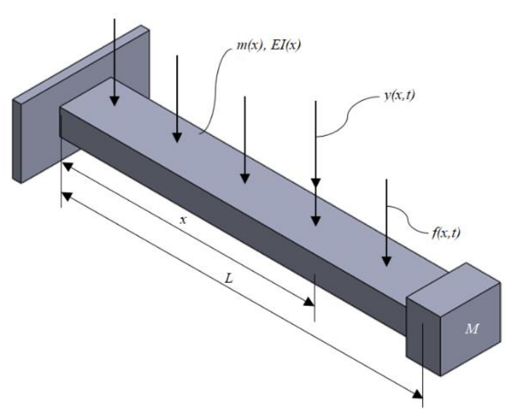

Figure 5. 9: *Cantilever beam having a lumped mass at its free end.*

5.2.3.1.1 Solution to the Link Arm’s Eigenvalue Problem

The Rayleigh’s quotient for the fixed-free prismatic cantilever beam in figure 5.9 which has a lumped mass at $x = L$ and is experiencing bending due to transversal vibrations, can be expressed in the form given in equation 5.4.

$$R(Y) = \lambda = \omega^2 = \frac{\frac{1}{2}\int_0^L EI(x)\left[\frac{\partial^2 Y(x)}{\partial x^2}\right]^2 dx}{\frac{1}{2}\int_0^L m(x)Y^2(x)dx+\frac{1}{2}MY^2(L)} \tag{5.4}$$

For this system, each finite element of the beam has the 4×4 stiffness and mass matrices given in equation 5.5 and 5.6, which were formulated by using third-order interpolation functions along with integrals in the numerator and the denominator of the Rayleigh’s quotient expression given in equation 5.4.

$$K_j = \frac{EI_j n^3}{L^3}\begin{bmatrix} 12 & 6 & -12 & 6 \\ 6 & 4 & -6 & 2 \\ -12 & -6 & 12 & -6 \\ 6 & 2 & -6 & 4 \end{bmatrix} \tag{5.5}$$

$$M_j = \frac{m_j L}{420n}\begin{bmatrix} 156 & 22 & 54 & -13 \\ 22 & 4 & 13 & -3 \\ 54 & 13 & 156 & -22 \\ -13 & -3 & -22 & 4 \end{bmatrix} + MY^2(L) \tag{5.6}$$

Just as in Chapter 3, the eigenvalue problem was evaluated with a computer code written in MATLAB scientific computer language to obtain the natural frequencies and modes of vibration occurring in the equivalent link arm beam. The approximate eigenvalues obtained with this code can be applied to any arbitrary prismatic fixed-free cantilever beam with a lumped mass at its free end. In order to compute the fundamental natural radial frequency for the link arm as given in equation 4.48, the magnitude of the lumped mass, as well as the link arm's geometrical and natural parameters were sought from the robot's CAD model.

It was easy to obtain the *'lumped mass'* from the CAD model to be 40.2622Kg. When inputted into the MATLAB program which can be found in Appendix B2, the approximate lowest eigenvalue, λ_1 of the system was obtained to be 0.8390. However, in order to carry out an acceptable approximate solution from the mathematical model, a more challenging task arose due to the non-uniform geometrical characteristics of the link arm. As it can be seen in figure 5.10, the cross-section of link arm has a hollow mid-section and a non-uniform external feature. This makes it tricky to obtain the appropriate parameters to use in equation 4.48 for evaluating the natural radial frequencies of vibration.

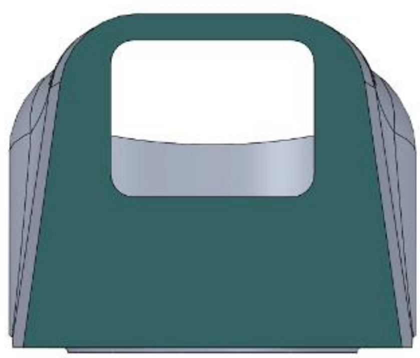

Figure 5. 10: *Cross-sectional profile of the robot's link arm geometry.*

For an acceptable approximation to be obtained, the parameters such as the mass, modulus of elasticity, length and second moment of area of the representative prismatic beam must all be excellent representations of the actual parameters on the non-uniform hollow link arm. To solve this problem, a technique was adopted which leveraged on the utilities which integrated CAE provides. The procedure which was followed in order to obtain a uniform beam to represent the non-uniform link arm has been outlined below.

a. The length, $L = 650mm$ was assigned to the equivalent beam as it was obtained from the CAD model of the link arm.

b. The cross-section of the link arm in figure 5.10 was measured in order to obtain an approximate cross-section in figure 5.11 for the representative beam which was used in the mathematical model. The external sides of the cross-section were assigned the values $A = 146.93mm$ and $B = 136.93mm$, while the inner cut-out was assigned $a = 70mm$ and $b = 88mm$, which were all approximated from the actual link-arm cross-section.

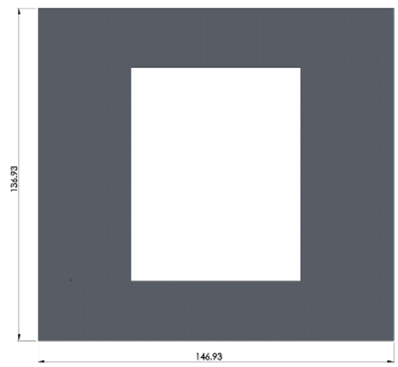

Figure 5. 11: *Cross-section of the link arm equivalent beam's geometry.*

c. To ensure that the beam is a good approximation, its natural parameters which include its stiffness and mass had to be equivalent to that of the link arm. The link arm, along with the other primary moving bodies of the robot had already been assigned Aluminium 6061 for its manufacture. The mass of the link arm was obtained from its CAD model to be $24.4918Kg$.

d. To obtain the mass, m a CAD model of the beam which is presented in figure 5.12 was created with the already determined geometrical parameters. After assigning Aluminium 6061 to it, which has a modulus of elasticity, $E = 69000MPa$, the beam model was found to have a mass, $m = 24.4983Kg$. This means that the link arm and the approximate beam have approximately the same mass with a negligible difference of 0.023%.

Figure 5. 12: *Link arm and its approximate representative beam's geometry.*

e. The final test, which is very important to ascertain the similarity between the two bodies had to do with their stiffness. To achieve this, a technique was adopted which required carrying out numerical simulations on both solid models. The steps taken and results obtained have been outlined below.

i. The goal was to compute the two bodies' resistance to deformation, which is given by their stiffness value, k. The mathematical relationship between force, F applied to a body, the displacement x which the body experiences, and the stiffness of the body is given below.

$$F = kx \tag{5.7}$$

ii. In order to figure out the stiffness of both bodies, a linear static structural analysis was carried out in SOLIDWORKS simulation.

iii. The simulation setup involved applying a fixture at the left end of the body's CAD model being simulated, and a transverse load was applied to the right end. For this simple simulation, a mesh was generated by the software without any specific mesh controls, and since it was sufficient the software was made to simulate the scenario. As it would be expected from the result, the bodies both experienced some bending away from the ideal centerline of their horizontal axis, as seen below.

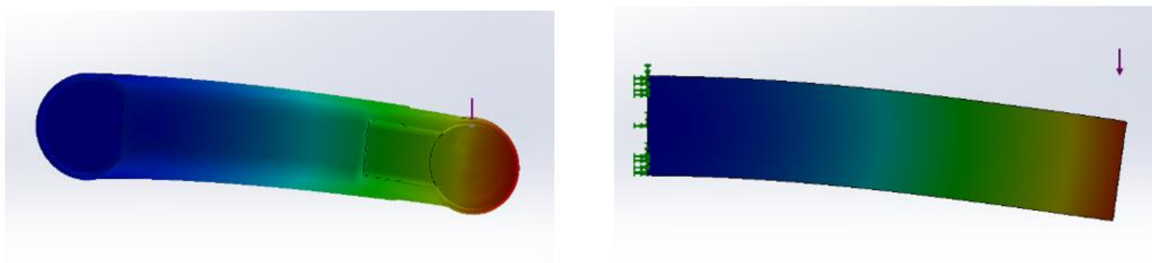

Figure 5. 13: *Graphical representation of displacements in link arm and approximate beam.*

iv. To aid with the stiffness computation, the same setup was carried out for six (6) scenarios with varied transversal loading, and a record of the maximum resultant displacement experienced by each of the bodies for each scenario can be found tabulated in figure 5.14.

Static Loading Scenarios

		1	2	3	4	5	6	Total
	Applied Force, F (N)	6000	6500	7000	7500	8000	10000	45000
Max Displacement, x (mm)	Link Arm	0.3203	0.347	0.3737	0.4004	0.4271	0.5339	2.4024
	Equivalent Beam	0.3179	0.3444	0.3709	0.3974	0.4239	0.5299	2.3844
	Difference (mm)	0.0024	0.0026	0.0028	0.003	0.0032	0.004	0.018
Stiffness, K (N/mm)	Link Arm	18732.44	18731.99	18731.6	18731.27	18730.98	18730.1	18731.27
	Equivalent Beam	18873.86	18873.4	18873.01	18872.67	18872.38	18871.49	18872.67
	Difference (N/mm)	141.4214	141.4145	141.4087	141.4036	141.3992	141.3859	141.4036
Avrg. Stiffness, K (N/mm)	Link Arm	18731.27						
	Equivalent Beam	18872.67		F = K*x				

Figure 5. 14: *Maximum resultant displacements under six (6) different loading scenarios.*

v. The results obtained and the graph plotted which has been presented in figure 5.15. show extreme closeness in the stiffness characteristics of the two bodies, since they both experience an almost equal amount of displacement when subjected to the same loading. The calculation presented below indicates that the absolute difference in the stiffness of both bodies is a very acceptable 0.7492%.

$$\% \, error = \left(\frac{18872.67 - 18731.27}{18872.67}\right) * 100 = 0.7492\% \qquad (5.8)$$

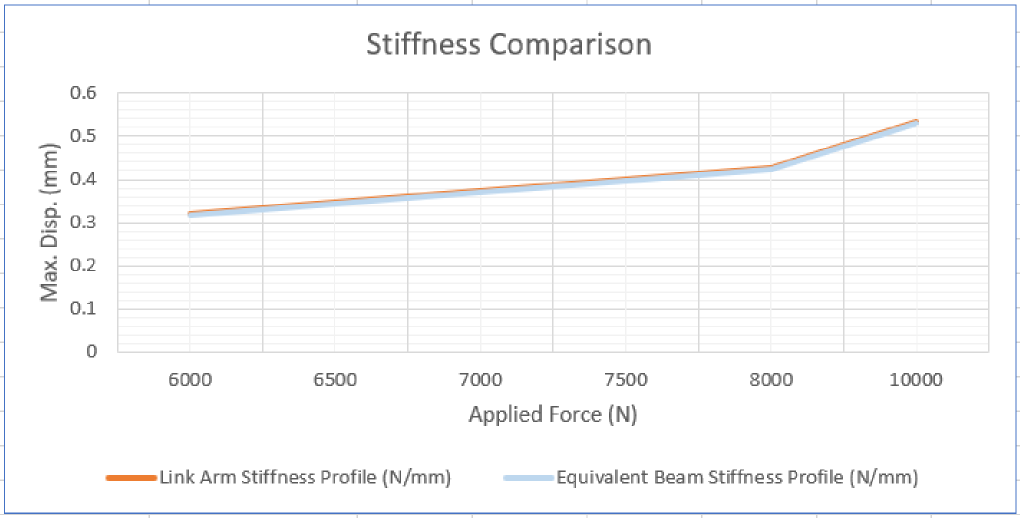

Figure 5. 15: *Stiffness comparison between the link arm and the approximate beam.*

f. With the difference in natural characteristics obtained to be negligibly small, it meant that the geometric parameters earlier assigned to the approximate beam were also acceptable and could therefore be used in the MATLAB code to mathematically evaluate the approximate fundamental natural frequency of the link arm in the prescribed configuration.

g. Referring to the MATLAB code which can be found in Appendix B2, the fundamental natural frequency was computed with the use of equation 4.48 to be $78.4745Hz$, which is sufficiently high for the actual robot's link arm. The plotted mode shapes for the first three modes of vibration can be found in figure 5.16.

$$f_1 = \frac{0.8390}{2\pi}\sqrt{\frac{EI}{mL^4}} = \frac{0.8390}{2\pi}\sqrt{\frac{(6.9*10^{10}N/m^2)*(3.3680*10^{-5}m^4)}{\left(\frac{24.4983}{0.65}Kg/m\right)*0.65^4m^4}} = 78.4745Hz \qquad (5.9)$$

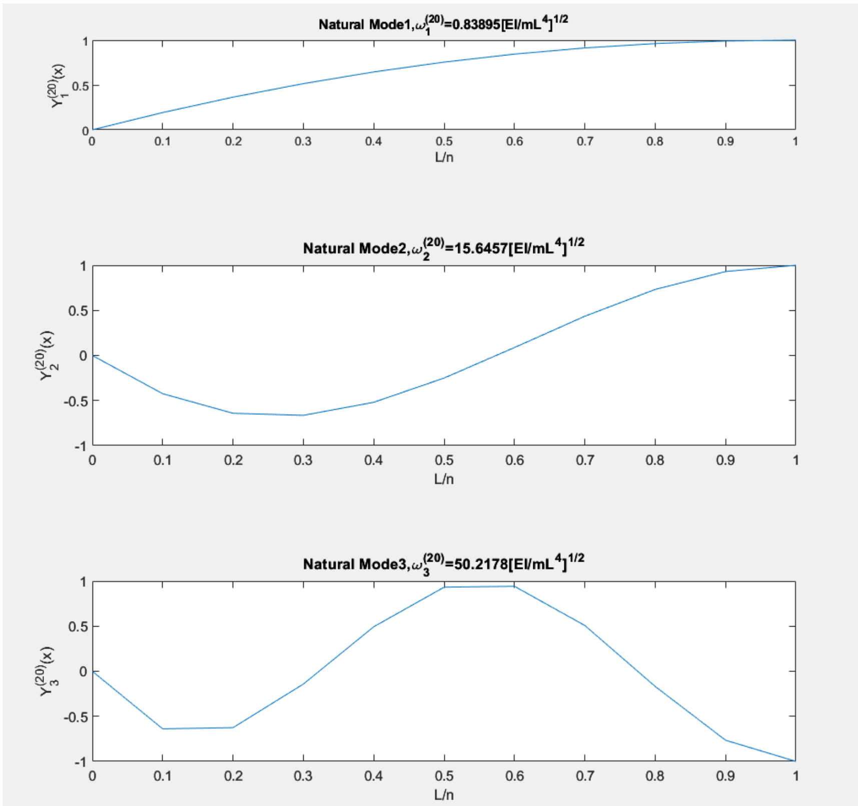

Figure 5. 16: *The first three (3) mode shapes of the vibrating beam.*

h. The lowest natural frequency of $78.4745Hz$ was obtained by using the actual lumped mass of $40.2622Kg$, however to aid further verification and to ascertain the effectiveness of this procedure, the lumped masses were reasonably varied to obtain different fundamental natural frequency values which have been presented in table 5.3. These values will be compared against their numerically obtained counterparts in the next section.

Table 5. 3: Natural Frequencies Obtained for Different Lumped Masses.

Lumped Mass, m *(Kg)*	40.26	50.00	60.00	70.00	80.00	100.00	200.00	500.00	1000.00
Fundamental Natural Frequency, f_1 *(Hz)*	78.48	70.80	64.88	60.23	56.45	50.64	36.02	22.86	16.18

5.2.3.2 Numerical Frequency Analysis

In this section, numerical analysis of the link arm is presented, along with comparison of the simulation tool's results against the analytical results which were presented above.

5.2.3.2.1 Simulation Study Setup

Similar to the steps outlined earlier, a model of the link arm which already had the Aluminium 6061 alloy material assigned to it was imported into SOLIDWORKS Simulation environment. The left end of the link was assigned a fixed boundary condition to simulate the locked state of the robot's joint q_2, while a remote mass of $40.2622 Kg$ was assigned to its right end which represents the equivalent mass of all the links and motors connected to the robot's joint q_3.

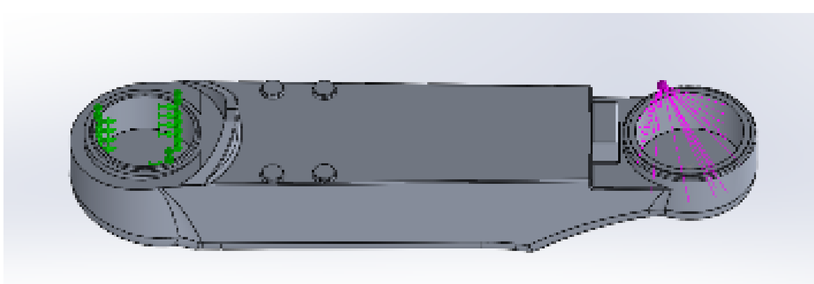

Figure 5. 17: *Setup of the link arm for frequency simulation.*

5.2.3.2.2 Simulation Results

With the setup achieved, the simulation tool was made to execute the analysis. The primary interest was in the lowest or fundamental natural frequency of vibration of the link arm under the prescribed configuration. This important value was obtained from the simulation tool's results to be $78.3760Hz$, and the scaled-up mode shape of the link arm which can be seen below in figure 5.18 indicates that it is experiencing a bending in the vertical plane, starting from joint q_3 towards joint q_2 of the robot.

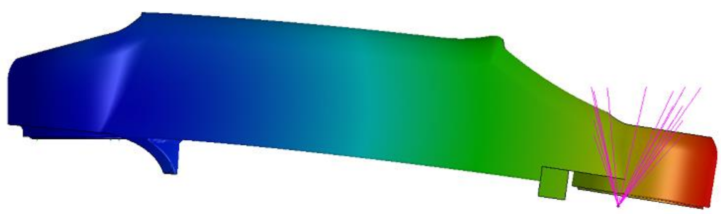

Figure 5. 18: *Graphical representation of the link arm's fundamental mode of vibration.*

This lowest natural frequency is sufficient for the link arm. However, to verify the accuracy of this computer-aided numerical analysis result it was compared against the $78.4745Hz$ which was obtained with mathematical modelling during analytical hand computation.

$$\%\ error = \left(\frac{78.4745Hz - 78.3760Hz}{78.4745Hz}\right) * 100 = 0.1255\% \qquad (5.10)$$

5.3 Summary and Discussion

Within the scope of this study, not much optimization was required to be carried out on the robot's structure. Only slight modifications were done during the static structural analysis, such as modifying the base of the robot in order to distribute stresses from a region of high stress concentration to neighboring regions of the base.

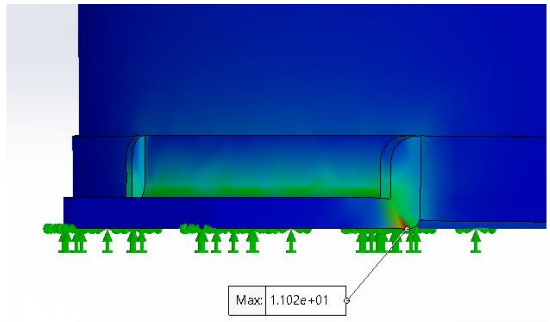

Figure 5. 19: *Region of maximum stress on the robot's base after an initial simulation.*

During an initial static structural simulation on configuration one (1) a maximum stress of $11Mpa$ was discovered on a region of the base. This raised concerns; hence some geometrical modification was done to the base, which can be found in figure 5.20. This structural optimization greatly reduced the stresses on the base of the robot, and the resulting maximum stress on the overall structure reduced to $6.58MPa$ for configuration one (1).

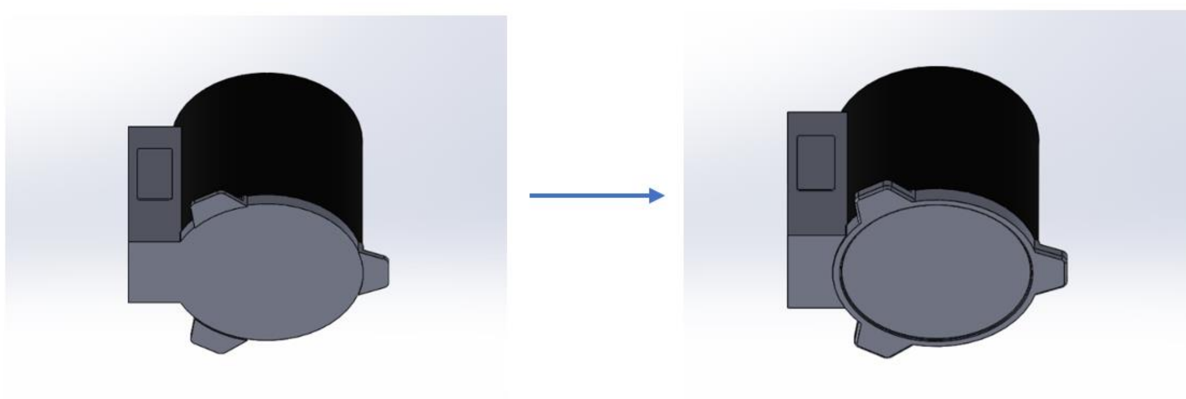

Figure 5. 20: *Optimization of the robot base's geometry.*

It is important to keep in mind that analytical vibration modelling presented above an approximation procedure with which to obtain an estimate of what the simulation tool's numerical results should be. The result presented, where the actual lumped mass of $40.2622Kg$ was used indicates a difference of 0.1255%, which is negligible. However, in order to further verify the effectiveness of the procedure more simulations ware carried out with different lumped mass values and compared against results which were obtained from the MATLAB code in Appendix B2. From the data tabulated in figure 5.21, it can be observed that the differences in the result for each scenario with a different lumped mass, between the numerical and the analytical cases is very minimal and negligible for lumped masses in the same order of magnitude as the real lumped mass.

However, as the order of magnitude of the lumped mass is increased, a wider difference which is still considerably minimal can be noticed. It should be noted that for this system, the higher order of magnitude lumped masses are impracticable and are only used as a means to show the effectiveness of the analytical approximation approach which has been presented in this study. In practice, the sum total of the mass of links, motors and loading which will be subjected to joint j_3 of the robot (at the right end of the link arm) should not be unreasonably high since this will cause the link arm structure to fail. Furthermore, in the case where it is structurally practicable, it will require the robot to have a very massive motor at joint j_3, which is not desirable.

		Trial Mass Values							
	Actual	1	2	3	4	5	6	7	8
Lumped Mass *(Kg)*	40.262	50	60	70	80	100	200	500	1000
	Fundamental Natural Frequency *(Hz)*								
Numerical Result	78.376	71.177	65.523	61.032	57.354	51.634	37.001	23.601	16.751
Analytical Result	78.475	70.803	64.878	60.229	56.454	50.639	36.016	22.858	16.182
Difference	0.0985	0.3742	0.6447	0.8033	0.8999	0.9946	0.9854	0.7426	0.5687
Approx. % Error	0%	1%	1%	1%	2%	2%	3%	3%	3%

Figure 5. 21: *Fundamental natural frequency comparisons for different lumped masses.*

The results from these comparisons confirm that the analytical technique carried out earlier offers a useful means of verifying the numerical results for analyses of this kind. Although the focus was on the link arm due to its critical location in the center of the robotic structure, the mathematical modelling procedure which is presented in this study, as well as the approximation technique deployed can also serve as a basis which can be expanded to make analytical hand computations for the dynamic behavior of any serial-linked robot's structure.

To answer the main research questions which were posed at the beginning of the study, the results from the computer-aided static structural and frequency analyses which were carried out on the robot model indicates that for any configuration of the robot, the link arm, and other links in the robot as a whole are strong and stiff enough to withstand static and dynamic loading within the recommended maximum loading capacity and loading distribution. Vibrations experienced in its links during operation will be minimal and have very minor influence on the robot's dynamic accuracy upon experiencing different kinds of loading which are within what has been recommended. Furthermore, the numerical results which were obtained from frequency analysis agreed very closely with the analytical results, indicating the accuracy of the numerical results and the validity of the analytical modelling procedure. In summary, the design meets all design objectives including excellent structural rigidity and high natural frequency. There might also be some opportunities to further reduce the weight of the structure, and this can be realized by carrying out a topology study.

Conclusion

To achieve a structural design for an industrial robot which is optimal, the links of the robot and its joints should have significant stiffness so as to ensure that it can resist vibrations that are capable of negatively influencing the robot's ability to achieve excellent levels of accuracy. Using a stiff material can help in achieving this, however high stiffness comes with high weight. Considering that the engineer needs to be mindful of the weight constraints of the robot when designing, the CAE and verification procedures which have been presented in this study offers an effective means with which to make informed design decisions regarding the geometrical and natural parameters of the robotic structure's component bodies.

For this study, the complete robotic system has been modelled and numerically analyzed with an integrated CAE tool, while one of the links was isolated for an in-depth study of its dynamical behaviors, involving both numerical analysis with the computational tool and verification by means of analytical mathematical modelling. As indicated by the analyses results of this study, if the design engineer can obtain a natural frequency for the first mode of vibration of the system which is sufficiently high, then by isolating the robot's operating environment from frequencies lower than or equal to this fundamental natural frequency, s/he can be rest assured that the system's structure is stiff enough and that resonance will not occur in the system. It is important to note that for a robotic structure design such as this, avoiding resonance alone is not enough. Since the system needs to be characterized by high accuracy capability, an even higher fundamental frequency of vibration is required to help the robotic system in avoiding minor vibrations which could still negatively affect its accuracy levels while in operation.

All the major geometrical features such as shape, length and thickness of the links were maintained after all the analyses were conducted. For future work however, a topology study is proposed with which more in-depth investigation can be carried out in order to identify regions of the robot where material utilization can be reduced through geometrical modifications. This is in a bid to better satisfy the requirement of lightweight construction as well as low-cost construction. In this future study, care must be taken to ensure that the robot maintains its excellent structural characteristics, including its high natural frequencies of vibration.

References

[1] Goel R., Gupta P. (2020): Robotics and Industry 4.0. in: Nayyar A., Kumar A. (eds) A Roadmap to Industry 4.0: Smart Production, Sharp Business and Sustainable Development. Advances in Science, Technology & Innovation (IEREK Interdisciplinary Series for Sustainable Development). Springer, Cham, pp.157-169, DOI https://doi.org/10.1007/978-3-030-14544-6_9, Print ISBN 978-3-030-14543-9, Online ISBN 978-3-030-14544-6 https://link.springer.com/chapter/10.1007/978-3-030-14544-6_9

[2] "Industry 4.0: the fourth industrial revolution – guide to Industrie", available from: https://www.i-scoop.eu/industry-4-0/ (assessed on 22nd April, 2020)

[3] KUKA Roboter GmbH: Robot KR15/2 Technical Data, Augsburg, 1998. PP.9-33

[4] Bruno S., Oussama K. (Eds) (2016): *Springer Handbook of Robotics*. 2016, 2nd ed, Springer-Verlag, Berlin, pp. 400-743. ISBN: 978-3-319-32550-7, e-ISBN: 978-3-319-32552-1, DOI 10.1007/978-3-319-32552-1

[5] Angeles J. (2014): *Fundamentals of Robotic Mechanical Systems: Theory, Methods and Algorithms*, 4th ed, Springer Cham, New York, pp. 150-151. ISBN:978-3-319-01851-5, DOI:10.1007/978-3-319-01851-5

[6] J.-Y. K'Nevez, M. Cherif, M. Zapciu, and A. Gérard, *"Experimental Characterization of Robot Arm Rigidity in Order to Be Used in Machining Operation,"* vol. 5, pp. 5–8, 2012, [Online]. Available: http://arxiv.org/abs/1201.4445.

[7] V. D. Hunt, "Robot Manipulators," *Smart Robot.*, pp. 226–259, 1985, doi: 10.1007/978-1-4613-2533-8_6.

[8] B. W. Mooring, Z. S. Roth and M. R. Driels (1993), *"Fundamentals of manipulator calibration," Automatica*, vol. 29, no. 4. Pergamon, pp. 1151–1153, Jul. 01, 1993, doi: 10.1016/0005-1098(93)90119-E.

[9] F. T. Paziani, B. Di Giacomo, and R. H. Tsunaki, *"Robot measuring form errors," Robot. Comput. Integr. Manuf.*, vol. 25, no. 1, pp. 168–177, Feb. 2009, doi: 10.1016/j.rcim.2007.11.003.

[10] Á. Cservená and K. T. Szabó, *"Accuracy Measurements of Industrial Robots 2 . Kinematical description of the robots,"* Advanced Logistic Systems, vol. 9, no. 1, pp.

73–80, 2015.

[11] Li Zheng J. (2015): *"CAD, 3D Modeling, Engineering Analysis, and Prototype Experimentation- Industrial and Research Applications,"* Springer Cham, New York pp.85-128, ISBN:978-3-319-05920-4, ISBN:978-3-319-05921-1(eBook), DOI 10.1007/978-3-319-05921-1

[12] Philip A. L. (1999): *Comprehensive Dictionary of Electrical Engineering*, Springer-Verlag, Heidelberg, p. 186, ISBN:3-540-64835-6

[13] Tarun P., Suresh P, Swet C. (2017): *"Forward and Inverse Kinematic Analysis of Robotic Manipulators,"* International Research Journal of Engineering and Technology (IRJET) 04(02), p.1462, e-ISSN: 2395-0056, p-ISSN: 2395-0072

[14] Corke P.: Robotics Masterclass, QUT Robot Academy, Queensland University of Technology, Brisbane, available from: https://robotacademy.net.au/ (assessed on 10th November, 2019)

[15] M. J. D. Hayes and P. L. O. Leary, *"Kinematic Calibration Procedure for Serial Robots with Six Revolute Axes,"* pp. 1–27, 2001.

[16] H. Chih-Ching, K. Chin-Hsing, M. Daisuke, and T. Yukio, *Advances in Mechanism and Machine Science*, vol. 73, no. 16. 2019.

[17] Kumar V.: *Introduction to Robot Geometry and Kinematics*, University of Pennsylvania lecture notes p.22

[18] John J. C. (2005): *Introduction to Robotics: Mechanics and Control*, 3rd ed., Pearson Education International, London, pp.180-188, ISBN: 0-13-123629-6

[19] M. Bottin, S. Cocuzza, N. Comand, and A. Doria, *"Modeling and identification of an industrial robot with a selective modal approach," Appl. Sci.*, vol. 10, no. 13, 2020, doi: 10.3390/app10134619.

[20] A. Pashkevich, A. Klimchik, D. Chablat, *"Enhanced stiffness modeling of manipulators with passive joints," Mechanism and Machine Theory*, vol. 46, 2011, pp. 662-679

[21] M. Bhusnar and S. S. Sarawade, *"Modal Analysis of Rectangular Plate with Lap Joints to Find Natural Frequencies and Mode Shapes,"* no. March, pp. 6–14, 2016.

[22] Meirovitch L. (2001): *Fundamentals of Vibrations*, McGraw-Hill, Singapore, pp. 383-600. ISBN:0-07-041345-2

[23] M. Bugday and M. Karali, *"Design optimization of industrial robot arm to minimize*

redundant weight," Eng. Sci. Technol. an Int. J., vol. 22, no. 1, pp. 346–352, 2019, doi: 10.1016/j.jestch.2018.11.009.

[24] C. Pupaza, G. Constantin, and Ș. Negrila, *"Computer aided engineering of industrial robots,"* vol. 9, no. 2, pp. 87–92, 2014.

[25] M. Akdag (2008), *"Design and analysis of robot manipulators by integrated CAE procedures".* Dokuz Eylul University, pp. 20.

[26] A. Demirci (2012), *"Design and analysis of a SCARA robot"*. Dokuz Eylul University, pp. 21.

[27] R. Arora and S. Dhami, *"Finite element analysis and multibody dynamics of 6-DOF industrial robot,"* International Journal of Mechanical and Production Engineering and Research Development (IJMPERD) 07(05), p.1-12, e-ISSN: 2249-8001, p-ISSN: 2249-6890

Appendix A1

The homogeneous transformation matrix which defines the robot's froward kinematics:

$$ {}^{0}T_6 = \begin{bmatrix} r_{x1} & r_{x2} & r_{x3} & t_x \\ r_{y1} & r_{y2} & r_{y3} & t_y \\ r_{z1} & r_{z2} & r_{z3} & t_z \\ 0 & 0 & 0 & 1 \end{bmatrix} \tag{4.16} $$

The complete expressions for the elements of the homogeneous transformation matrix:

$$ r_{x1} = s_6\big(c_4s_1 - s_4(c_1c_2c_3 - c_1s_2s_3)\big) + c_6\big(c_5\big(s_1s_4 + c_4(c_1c_2c_3 - c_1s_2s_3)\big) - s_5(c_1c_2s_3 + c_1c_3s_2)\big) \tag{4.16a} $$

$$ r_{x2} = c_6\big(c_4s_1 - s_4(c_1c_2c_3 - c_1s_2s_3)\big) - s_6\big(c_5\big(s_1s_4 + c_4(c_1c_2c_3 - c_1s_2s_3)\big) - s_5(c_1c_2s_3 + c_1c_3s_2)\big) \tag{4.16b} $$

$$ r_{x3} = s_5\big(s_1s_4 + c_4(c_1c_2c_3 - c_1s_2s_3)\big) + c_5(c_1c_2s_3 + c_1c_3s_2) \tag{4.16c} $$

$$ t_x = c_1(300 + 650c_2 + 140s_5c_4(c_2c_3 - s_2s_3) + 140c_5(c_2s_3 + c_3s_2) + 155(c_2c_3 - s_2s_3) + 600(c_2s_3 + c_3s_2)) + 140s_1s_4s_5 \tag{4.16d} $$

$$ r_{y1} = -s_6\big(c_1c_4 - s_4(s_1s_2s_3 - s_1c_2c_3)\big) - c_6\big(c_5\big(c_1s_4 + c_4(s_1s_2s_3 - s_1c_2c_3)\big) + s_5(s_1c_2s_3 + s_1s_2c_3)\big) \tag{4.16e} $$

$$ r_{y2} = s_6\big(c_s\big(c_1s_4 + c_4(s_1s_2s_3 - s_1c_2c_3)\big) + s_5(s_1c_2s_3 + s_1s_2c_3)\big) - c_6(c_1c_4 - s_4(s_1s_2s_3 - s_1c_cc_3)) \tag{4.16f} $$

$$ r_{y3} = c_5(s_1c_2s_3 + s_1s_2c_3) - s_5(c_1s_4 + c_4(s_1s_2s_3 - s_1c_2c_3)) \tag{4.16g} $$

$$ t_y = s_1(300 + 650c_2 - 140s_5c_4(s_2s_3 - c_2c_3) + 140c_5(c_2s_3 + c_3s_2) + 155(c_2c_3 - s_2s_3) + 600(c_2s_3 + c_3s_2)) - 140c_1s_4s_5 \tag{4.16h} $$

$$ r_{z1} = c_6\big(s_5(c_2c_3 - s_2s_3) + c_4c_5(c_2s_3 + c_3s_2)\big) - s_4s_6(c_2s_3 + c_3s_2) \tag{4.16i} $$

$$ r_{z2} = -s_6\big(s_5(c_2c_3 - s_2s_3) + c_4c_5(c_2s_3 + c_3s_2)\big) - s_4c_6(c_2s_3 + c_3s_2) \tag{4.16j} $$

$$ r_{z3} = c_4s_5(c_2s_3 + s_2c_3) - c_5(c_2c_3 - s_2s_3) \tag{4.16k} $$

$$ t_z = 650s_2 - 600c_2c_3 + 155c_2s_3 + 155c_3s_2 + 600s_2s_3 - 140c_5\big(c_2c_3 - s_2s_2) + 140c_4s_5(c_2s_3 + c_3s_2)\big) + 675 \tag{4.16l} $$

Where, $c_i = \cos(q_i)$ and $s_i = \sin(q_i)$.

Appendix A2

```
% Industrial Robot Structure Design

% For the industrial robotic manipulator designed in this study, this code computes:
% - The forward kinematics,
% - The Jacobian matrix at two configurations of the robot, and
% - The robot's links center of mass velocities.

%%
% Forward Kinematics (Homogeneous Transformation Matrices)

% Symbolic variables that represent the six (6) individual transformation matrices
syms T0_1 T1_2 T2_3 T3_4 T4_5 T5_6
% Symbolic variables that represent the six (6) joints (generalized coordinates)
syms Research_Robot_FKM(q1, q2, q3, q4, q5, q6)

% Generate the D-H parameters table for the Robot
% The robotics toolbox is very well set-up to deal with Denavit-Hartenberg notation.
% Create a D-H matrix and each row in this matrix represents a single link.

% 6 X 4 matrix which contains the D-H parameters for the 6-joint robot.
Research_Robot_DH = [0 0.675 0.300 1.5708;
                     0 0 0.650 0;
                     0 0 0.155 1.5708;
                     0 0.600 0 -1.5708;
                     0 0 0 1.5708;
                     0 0.140 0 0];

% A robot object is created, and put it into the workspace variable Research_Robot
% The D-H parameter matrix is passed into toolbox function 'SerialLink'

% The result is a serial link object which represents the robot arm, created in MATLAB
workspace.
Research_Robot = SerialLink(Research_Robot_DH, 'name', 'Research Robot');

% When run, the D-H parameters are displayed in table form in the command window.

% Once this object has been obtained, simple functions can be performed on it.
% Two configurations of the robot are plotted below

% Only the second joint angle is 1.5708 radians (90 deg.) and all others are locked at 0 degrees.
% Research_Robot.plot([0 1.5708 0 0 0 0]);
% Research_Robot.plot([0 0 1.5708 0 0 0]);
% A teach pendant is created, which displays the location of the robot's end-effector
% The teach pendant, brings up the sliders which allows movement of the robotic arm's joints.
```

```
% Research_Robot.teach([0 1.5708 0 0 0 0]);
% Research_Robot.teach([0 0 1.5708 0 0 0]);

%%
% Direct (analytical) Computation
% General form of each Homogeneous Transformation Matrix for revolute joints robot

%Ti-1_i =[cos(q_i) -(sin(q_i)*(cos(alpha_i))  sin(q_i)*sin(alfa_i)  a_i*cos(q_i);
%        sin(q_i)   cos(q_i)*cos(alpha_i)  -(cos(q_i)*sin(alfa_i))  a_i*sin(q_i);
%        0          sin(alfa_i)             cos(alpha_i)          d_i;
%        0          0                       0                     1]

% Compute the forward kinematics:
% Substitute parameters from the D-H table for each link
% Multiply the six(6) transformation matrices

T0_1 = [cos(q1) 0 sin(q1) 0.300*cos(q1);
        sin(q1) 0 -cos(q1) 0.300*sin(q1);
        0 1 0 0.675;
        0 0 0 1];

T1_2 = [cos(q2) -sin(q2) 0 0.650*cos(q2);
        sin(q2) cos(q2) 0 0.650*sin(q2);
        0 0 1 0;
        0 0 0 1];

T2_3 = [cos(q3) 0 sin(q3)  0.155*cos(q3);
        sin(q3) 0 -cos(q3) 0.155*sin(q3);
        0 1 0 0;
        0 0 0 1];

T3_4 = [cos(q4) 0 -sin(q4) 0;
        sin(q4) 0 cos(q4) 0;
        0 -1 0 0.600;
        0 0 0 1];

T4_5 = [cos(q5) 0 sin(q5) 0;
        sin(q5) 0 -cos(q5) 0;
        0 1 0 0;
        0 0 0 1];

T5_6 = [cos(q6) -sin(q6) 0 0;
        sin(q6) cos(q6) 0 0;
        0 0 1 0.140;
        0 0 0 1];
```

```
% Multiply the 6 transformation matrices in order to obtain the single FK matrix
syms Research_Robot_FKMatrix;

Research_Robot_FKM(q1, q2, q3, q4, q5, q6) = T0_1 * T1_2 * T2_3 * T3_4 * T4_5 * T5_6;
Research_Robot_FKMatrix = T0_1 * T1_2 * T2_3 * T3_4 * T4_5 * T5_6;

% Extracted x,y and z coordinates of the robot EE's position:
KUKA_EE_x = Research_Robot_FKMatrix(1,4);
KUKA_EE_y = Research_Robot_FKMatrix(2,4);
KUKA_EE_z = Research_Robot_FKMatrix(3,4);

% Substitute some real angle values (inputs) into the FK matrix
% Angle values for the two chosen configurations position:

% Only angle q2 = 90deg (in radians)
Research_Robot_Pose1 = double(Research_Robot_FKM(0, 1.5708, 0, 0, 0, 0));
% Only angle q3 = 90deg (in radians) - maximum reach
Research_Robot_Pose2 = double(Research_Robot_FKM(0, 0, 1.5708, 0, 0, 0));

%%
% Verification of the result using Robotics Toolbox object:

% The robot object also has a forward kinematic method, 'fkine' which can be applied to it.
% When the different joint angles for each of the configurations that are being treated
% are passed into the 'fkine' method, it will return a homogeneous transformation representing
% the pose of the robot's end-effector for the respective configurations.

% Only angle q2 = 90deg (in radians)
Research_Robot_Ver1 = Research_Robot.fkine([0 1.5708 0 0 0 0]);
% Only angle q2 = 90deg (in radians) - maximum reach
Research_Robot_Ver2 = Research_Robot.fkine([0 0 1.5708 0 0 0]);

% The first 3x3 elements represent the orientation of the robot's end-effector.
% The last 3x1 are the x, y and z coordinates of the robot's end-effector position.

%%
% Jacobian
% Rows 1-3: translational velocities of the robot's EE at the selected configuration.
% Rows 4-6: angular velocities of the robot's EE at the selected configuration.

J1 = KUKA_KR15_2.jacobe([0 1.5708 0 0 0 0]); % Only angle q2 = 90deg (in radians)
J2 = KUKA_KR15_2.jacobe([0 0 1.5708 0 0 0]); % Only angle q2 = 90deg (in radians) -
maximum reach

% Inverse Jacobian
% The Jacobian at a specific configuration is not invertible if its determinant is equal to zero.
```

```
% Both are not invertible, hence they are singular Jacobian matrices.
det(J1);
det(J2);
% inv(J1);
% inv(J2);

%%
% Dynamics - Computing velocity of links centers of mass
syms q1_dot q2_dot q3_dot q4_dot q5_dot q6_dot;

u_1_1 = [0 -1 0 0; 1 0 0 0; 0 0 0 0; 0 0 0 0] * T0_1;
v_c_1 = (u_1_1 * q1_dot) * [0.1662; 0.0023; 0.1460; 1];

u_2_1 = [0 -1 0 0; 1 0 0 0; 0 0 0 0; 0 0 0 0] * T0_1 * T1_2;
u_2_2 = T0_1 * [0 -1 0 0; 1 0 0 0; 0 0 0 0; 0 0 0 0] * T1_2;
v_c_2 = ((u_2_1 * q1_dot) + (u_2_2 * q2_dot)) * [0.0000; 0.3067; 0.0479; 1];

u_3_1 = [0 -1 0 0; 1 0 0 0; 0 0 0 0; 0 0 0 0] * T0_1 * T1_2 * T2_3;
u_3_2 = T0_1 * [0 -1 0 0; 1 0 0 0; 0 0 0 0; 0 0 0 0] * T1_2 * T2_3;
u_3_3 = T0_1 * T1_2 * [0 -1 0 0; 1 0 0 0; 0 0 0 0; 0 0 0 0] * T2_3;
v_c_3 = ((u_3_1 * q1_dot) + (u_3_2 * q2_dot) + (u_3_3 * q3_dot)) * [-0.1823; -0.0428; 0.0033;
1];

u_4_1 = [0 -1 0 0; 1 0 0 0; 0 0 0 0; 0 0 0 0] * T0_1 * T1_2 * T2_3 * T3_4;
u_4_2 = T0_1 * [0 -1 0 0; 1 0 0 0; 0 0 0 0; 0 0 0 0] * T1_2 * T2_3 * T3_4;
u_4_3 = T0_1 * T1_2 * [0 -1 0 0; 1 0 0 0; 0 0 0 0; 0 0 0 0] * T2_3 * T3_4;
u_4_4 = T0_1 * T1_2 * T2_3 * [0 -1 0 0; 1 0 0 0; 0 0 0 0; 0 0 0 0] * T3_4;
v_c_4 = ((u_4_1 * q1_dot) + (u_4_2 * q2_dot) + (u_4_3 * q3_dot) + (u_4_4 * q4_dot)) * [-
0.1259; 0.0002; -0.0245; 1];

u_5_1 = [0 -1 0 0; 1 0 0 0; 0 0 0 0; 0 0 0 0] * T0_1 * T1_2 * T2_3 * T3_4 * T4_5;
u_5_2 = T0_1 * [0 -1 0 0; 1 0 0 0; 0 0 0 0; 0 0 0 0] * T1_2 * T2_3 * T3_4 * T4_5;
u_5_3 = T0_1 * T1_2 * [0 -1 0 0; 1 0 0 0; 0 0 0 0; 0 0 0 0] * T2_3 * T3_4 * T4_5;
u_5_4 = T0_1 * T1_2 * T2_3 * [0 -1 0 0; 1 0 0 0; 0 0 0 0; 0 0 0 0] * T3_4 * T4_5;
u_5_5 = T0_1 * T1_2 * T2_3 * T3_4 * [0 -1 0 0; 1 0 0 0; 0 0 0 0; 0 0 0 0] * T4_5;
v_c_5 = ((u_5_1 * q1_dot) + (u_5_2 * q2_dot) + (u_5_3 * q3_dot) + (u_5_4 * q4_dot) + (u_5_5
* q5_dot)) * [0.0288; 0.0000; 0.0691; 1];

u_6_1 = [0 -1 0 0; 1 0 0 0; 0 0 0 0; 0 0 0 0] * T0_1 * T1_2 * T2_3 * T3_4 * T4_5 * T5_6;
u_6_2 = T0_1 * [0 -1 0 0; 1 0 0 0; 0 0 0 0; 0 0 0 0] * T1_2 * T2_3 * T3_4 * T4_5 * T5_6;
u_6_3 = T0_1 * T1_2 * [0 -1 0 0; 1 0 0 0; 0 0 0 0; 0 0 0 0] * T2_3 * T3_4 * T4_5 * T5_6;
u_6_4 = T0_1 * T1_2 * T2_3 * [0 -1 0 0; 1 0 0 0; 0 0 0 0; 0 0 0 0] * T3_4 * T4_5 * T5_6;
u_6_5 = T0_1 * T1_2 * T2_3 * T3_4 * [0 -1 0 0; 1 0 0 0; 0 0 0 0; 0 0 0 0] * T4_5 * T5_6;
u_6_6 = T0_1 * T1_2 * T2_3 * T3_4 * T4_5 * [0 -1 0 0; 1 0 0 0; 0 0 0 0; 0 0 0 0] * T5_6;
v_c_6 = ((u_6_1 * q1_dot) + (u_6_2 * q2_dot) + (u_6_3 * q3_dot) + (u_6_4 * q4_dot) + (u_6_5
* q5_dot) + (u_6_6 * q6_dot)) * [0.0680; 0.0000; 0.0000; 1];
```

Appendix B1

```
% Preliminary_Analysis_with_Beam.m
% MATLAB program for the solution of the eigenvalue problem by FEM
% Computed based on [22]

% This program computes:
% - The natural frequencies and modes of vibration of a pinned-free prismatic beam with lumped mass at its free,
% - It plots the modes of vibration of the beam.

%%
clear
clf

n = 10; % number of finite elements
Ke = [12 6 -12 6; 6 4 -6 2; -12 -6 12 -6; 6 2 -6 4]*n^3; % element stiffness matrix (k)
Me = [156 22 54 -13; 22 4 13 -3; 54 13 156 -22; -13 -3 -22 4]/(420*n); % element mass matrix (m)

%%
% Constant stiffness and mass distribution over each element is assumed (i.e., constant axial rigidity and mass distribution)

% Stiffness distribution over the elements arranged in a n-dimensional vector
ke = [1 1 1 1 1 1 1 1 1 1];
% Mass distribution over the elements arranged in an n-dimensional vector
me = [1 1 1 1 1 1 1 1 1 1];

%%
% Generation of a connectivity array to place the element stiffness
% and mass matrices in the global stiffness and mass matrices

for k = 1:n,
   CA(k,1) = k;
   CA(k,2) = k+1;
end

%%
% Nulling the global K and M matrices before enforcement of the BCs
K1 = zeros (2*n+2, 2*n+2);
M1 = zeros (2*n+2, 2*n+2);

K = zeros (2*n, 2*n); % nulling the stiffness matrix
M = zeros (2*n, 2*n); % nulling the mass matrix
```

```
%%
% Assembly of the global matrices before enforcement of the boundary conditions
for k=1:n,
   for p=1:2,
      for q=1:2,
         K1(2*CA(k,p)-1, 2*CA(k,q)-1) = K1(2*CA(k,p)-1, 2*CA(k,q)-1)+ke(k) * Ke(2*p-1,
2*q-1);
         K1(2*CA(k,p)-1, 2*CA(k,q)) = K1(2*CA(k,p)-1, 2*CA(k,q))+ke(k) * Ke(2*p-1, 2*q);
         K1(2*CA(k,p), 2*CA(k,q)-1) = K1(2*CA(k,p), 2*CA(k,q)-1)+ke(k) * Ke(2*p, 2*q-1);
         K1(2*CA(k,p), 2*CA(k,q)) = K1(2*CA(k,p), 2*CA(k,q))+ke(k) * Ke(2*p, 2*q);

         M1(2*CA(k,p)-1, 2*CA(k,q) -1) = M1(2*CA(k,p)-1,  2*CA(k,q)-1)+me(k)*Me(2*p-1,
2*q-1);
         M1(2*CA(k,p)-1, 2*CA(k,q)) = M1(2*CA(k,p)-1, 2*CA(k,q))+me(k)*Me(2*p-1,2*q);
         M1(2*CA(k,p), 2*CA(k,q)-1) = M1(2*CA(k,p), 2*CA(k,q)-1)+me(k)*Me(2*p,2*q-1);
         M1(2*CA(k,p), 2*CA(k,q)) = M1(2*CA(k,p), 2*CA(k,q))+me(k)*Me(2*p, 2*q);
      end
   end
end

%%
% The left BC
for i=3:(2*n+2),
   for j=3:(2*n+2),
      K(i-2, j-2) = K1(i, j);
      M(i-2, j-2) = M1(i, j);
   end
end

% Beam is free at the right, hence there is no loop condition required

% Enforcement of the boundary conditions by retaining and relabeling the non-zero entries
K(2*n, 2*n) = K1(2*n+2, 2*n+2);
M(2*n, 2*n) = M1(2*n+2, 2*n+2);

%%
% Solution of the algebraic eigenvalue problem using MATLAB function eig()
% v = eigenvectors
% W = eigenvalues
[v,W] = eig(K, M);

%%
% Extracting the approximate eigenvalues and eigenvectors
for i=1:2*n,
   wl(i) = sqrt(W(i,i)); % natural frequencies arranged in a 2n-dimensional vector
```

```
%     for d=2:(2*n),
%        a = 1/sqrt(v(:,d)'*M*v(:,d)); % normalization factors
%        V(:,i) = a*v(:,i); % normalization of the eigenvectors
%     end
end

[w,I] = sort(wl); % arranging the natural frequencies in ascending order
for j=1:2*n,
   U1 (:,j)=v(:,I(j)); % arranging the modal vectors in ascending order
end

%%
% %%%%% Plotting mode shapes

for i=1:2*n,
   for j=1:2*n-1,
      U(i+1, j+1) = U1(i,j);
   end
end
%
for j=1:2*n-1,
   U(2*n+2, j+1) = U1(2*n, j);
   U(j+1, 2*n+2) = U1(j, 2*n);
end

U(2*n+2, 2*n+2) = U1(2*n, 2*n);

%%
s = [1:-1:0]; % local coordinate increments
% cubic interpolation functions
phi1 = 3*s.^2 - 2*s.^3;
phi2 = s.^2 - s.^3;
phi3 = 1 - 3*s.^2 + 2*s.^3;
phi4 = -s + 2*s.^2 - s.^3;

for m = 2:4,
   y = [ ];
   x = [ ];
   f = 0.1;
      if m >= 3;
         f = 0.2;
      end

   axes('position',[0.3 0.8-0.35*(m-2) 0.4 f]) % positioning of the plots in the workspace

   for k = 1:n,
```

```
        y1 = phi1 * U(2*CA(k,1)-1, m) + phi2 * U(2*CA(k,1), m) + phi3 * U(2*CA(k,2)-1, m) +
phi4 * U(2*CA(k,2), m);
        x1 = (k-s)/n;
        y = [y y1];
        x = [x x1];
    end

    plot(x,-y/max(abs(y)))
%     set(gca,'XTick',[0:0.1:1], 'XTickLabel','0|h||||||||10h')

    st = num2str(w(m-1));
    st1 = int2str(m-1);
    st2 = int2str(2*n);
    st3 = strcat('Y_', st1, '^{(',st2,')}(x)');
    st4 = strcat('Natural Mode', {''}, st1, {','}, '\omega_', st1, '^{(',st2,')}', '=', st,
'[EI/mL^4]^{1/2}');

    ylabel(st3)
    title(st4)
    xlabel('L/n')
end
```

Appendix B2

```
% Research_Robot_Link_Arm_with_Lumped_Mass.m
% MATLAB program for the solution of the eigenvalue problem by FEM.

% Computed based on [22].

% This program computes:
% - The natural frequencies and modes of vibration of a pinned-free prismatic beam with
lumped mass at its free,
% - It plots the modes of vibration of the beam.

%%
clear
% clf

n = 10; % number of finite elements

%actual lumped mass on the beam's free end
ml = 40.2622;

%randomly selected lumped masses for verification
% ml = 50;
% ml = 60;
% ml = 70;
% ml = 80;
% ml = 100;
% ml = 200;
% ml = 500;
% ml = 1000;

Lump = zeros (2*n+2, 2*n+2); % initialize lumped mass = 0 for the 11 nodes
Lump(19:2*n+2, 19:2*n+2) = [0 0 0 0; 0 0 0 0; 0 0 ml 0; 0 0 0 0]/n; % only the lumped mass
on the last node is equal to ml

Ke = [12 6 -12 6; 6 4 -6 2; -12 -6 12 -6; 6 2 -6 4]*n^3; % element stiffness matrix (k)
Me = [156 22 54 -13; 22 4 13 -3; 54 13 156 -22; -13 -3 -22 4]/(420*n); % element mass matrix
(m)

%%
% Constant stiffness and mass distribution over each element is assumed (i.e., constant axial
rigidity and mass distribution)

% Stiffness distribution over the elements arranged in a n-dimensional vector
ke = [1 1 1 1 1 1 1 1 1 1];
% Mass distribution over the elements arranged in an n-dimensional vector
```

```
me = [1 1 1 1 1 1 1 1 1 1];

%%
% Generation of a connectivity array to place the element stiffness
% and mass matrices in the global stiffness and mass matrices

for k = 1:n,
   CA(k,1) = k;
   CA(k,2) = k+1;
end

%%
% Nulling the global K and M matrices before enforcement of the BCs
K1 = zeros (2*n+2, 2*n+2);
M1 = zeros (2*n+2, 2*n+2) + Lump;

K = zeros (2*n, 2*n); % nulling the stiffness matrix
M = zeros (2*n, 2*n); % nulling the mass matrix

%%
% Assembly of the global matrices before enforcement of the boundary conditions
for k=1:n,
   for p=1:2,
      for q=1:2,
         K1(2*CA(k,p)-1, 2*CA(k,q)-1) = K1(2*CA(k,p)-1, 2*CA(k,q)-1)+ke(k) * Ke(2*p-1, 2*q-1);
         K1(2*CA(k,p)-1, 2*CA(k,q)) = K1(2*CA(k,p)-1, 2*CA(k,q))+ke(k) * Ke(2*p-1, 2*q);
         K1(2*CA(k,p), 2*CA(k,q)-1) = K1(2*CA(k,p), 2*CA(k,q)-1)+ke(k) * Ke(2*p, 2*q-1);
         K1(2*CA(k,p), 2*CA(k,q)) = K1(2*CA(k,p), 2*CA(k,q))+ke(k) * Ke(2*p, 2*q);

         M1(2*CA(k,p)-1, 2*CA(k,q) -1) = M1(2*CA(k,p)-1,  2*CA(k,q)-1)+me(k)*Me(2*p-1, 2*q-1);
         M1(2*CA(k,p)-1, 2*CA(k,q)) = M1(2*CA(k,p)-1, 2*CA(k,q))+me(k)*Me(2*p-1,2*q);
         M1(2*CA(k,p), 2*CA(k,q)-1) = M1(2*CA(k,p), 2*CA(k,q)-1)+me(k)*Me(2*p,2*q-1);
         M1(2*CA(k,p), 2*CA(k,q)) = M1(2*CA(k,p), 2*CA(k,q))+me(k)*Me(2*p, 2*q);
      end
   end
end

%%
% The left BC
for i=3:(2*n+2),
   for j=3:(2*n+2),
      K(i-2, j-2) = K1(i, j);
      M(i-2, j-2) = M1(i, j);
   end
```

```
end

% Beam is free at the right, hence there is no loop condition required

% Enforcement of the boundary conditions by retaining and relabeling the non-zero entries
K(2*n, 2*n) = K1(2*n+2, 2*n+2);
M(2*n, 2*n) = M1(2*n+2, 2*n+2);

%%
% Solution of the algebraic eigenvalue problem using MATLAB function eig()
% v = eigenvectors
% W = eigenvalues
[v,W] = eig(K, M);

%%
% Extracting the approximate eigenvalues and eigenvectors
for i=1:2*n,
   wl(i) = sqrt(W(i,i)); % natural frequencies arranged in a 2n-dimensional vector
   for d=2:(2*n),
      a = 1/sqrt(v(:,d)'*M*v(:,d)); % normalization factors
      V(:,i) = a*v(:,i); % normalization of the eigenvectors (modal vectors)
      % The eigenvectors represent the normal modes of vibration
   end
end

[w,I] = sort(wl); % arranging the natural frequencies in ascending order
for j=1:2*n,
   U1 (:,j)=V(:,I(j)); % arranging the modal vectors in ascending order
end

%%
% %%%%% Plotting the normal mode shapes

for i=1:2*n,
   for j=1:2*n,
      U(i+1, j+1) = U1(i,j);
   end
end

for j=1:2*n-1,
   U(2*n+2, j+1) = U1(2*n, j);
   U(j+1, 2*n+2) = U1(j, 2*n);
end

U(2*n+2, 2*n+2) = U1(2*n, 2*n);
```

```
%%
s = [1:-1:0]; % local coordinate increments
% cubic interpolation functions
phi1 = 3*s.^2 - 2*s.^3;
phi2 = s.^2 - s.^3;
phi3 = 1 - 3*s.^2 + 2*s.^3;
phi4 = -s + 2*s.^2 - s.^3;

for m = 2:4,
   y = [ ];
   x = [ ];
   f = 0.1;
   if m >= 3;
      f = 0.2;
   end

   axes('position',[0.3 0.8-0.35*(m-2) 0.4 f]) % positioning of the plots in the workspace

   for k = 1:n,
      y1 = phi1 * U(2*CA(k,1)-1, m) + phi2 * U(2*CA(k,1), m) + phi3 * U(2*CA(k,2)-1, m) +
phi4 * U(2*CA(k,2), m);
      x1 = (k-s)/n;
      y = [y y1];
      x = [x x1];
   end
   plot(x,-y/max(abs(y)))
%     set(gca,'XTick',[0:0.1:1], 'XTickLabel','0|h|2h|3h|4h|5h|6h|7h|8h|9h|10h')
%     set(gca,'XTick',[0:0.1:1], 'XTickLabel','0|h||||||||10h')
   st = num2str(w(m-1));
   st1 = int2str(m-1);
   st2 = int2str(2*n);
   st3 = strcat('Y_', st1, '^{(',st2,')}(x)');
   st4 = strcat('Natural Mode', {''}, st1, {','}, '\omega_', st1, '^{(',st2,')}', '=', st,
'[EI/mL^4]^{1/2}');

   ylabel(st3)
   title(st4)
   xlabel('L/n')
end

%%
% Natural frequency & frequency of vibration of the robot's link arm
L = 0.65; % m
A = 0.13693; % m
B = 0.14693; % m
a = 0.088; % m
```

```
b = 0.070; % m
In = ((A*B^3)/12)-((a*b^3)/12); % second moment of area (cross-sectional area moment of inertia) - m^4
m = 24.4983/L; % kg/m
E = 6.9*10^10; % Al 6061 modulus of elasticity - Pa - N/m^2
roh = 2700; % Al 6061, Pa - kg/m^3

Wn = w * sqrt((E*In)/(m*L^4));
fn = Wn/(2*pi);

%%
% Spring stiffness evaluation
% Forces (N) applied for each scenario
F1 = 6000;
F2 = 6500;
F3 = 7000;
F4 = 7500;
F5 = 8000;
F6 = 10000;
Total_F = F1+F2+F3+F4+F5+F6;

% Displacements (in mm) on link arm
a1 = 0.3203;
a2 = 0.3470;
a3 = 0.3737;
a4 = 0.4004;
a5 = 0.4271;
a6 = 0.5339;
Total_a = a1+a2+a3+a4+a5+a6;
K_link = Total_F/Total_a;

% Displacements (in mm) on equivalent beam in mm
b1 = 0.3179;
b2 = 0.3444;
b3 = 0.3709;
b4 = 0.3974;
b5 = 0.4239;
b6 = 0.5299;
Total_b = b1+b2+b3+b4+b5+b6;
K_beam = Total_F/Total_b;

Error = abs((K_link-K_beam)/K_link)*100;
Error2 = ((K_beam-K_link)/K_beam)*100;
```